WPMAT-PR(18) 21177

PW Ma et al.

# The universality of point defect structure in body-centred cubic metals

Preprint of Paper to be submitted for publication in
Physical Review Materials

This work has been carried out within the framework of the EUROfusion Consortium and has received funding from the Euratom research and training programme 2014-2018 under grant agreement No 633053. The views and opinions expressed herein do not necessarily reflect those of the European Commission.

This document is intended for publication in the open literature. It is made available on the clear understanding that it may not be further circulated and extracts or references may not be published prior to publication of the original when applicable, or without the consent of the Publications Officer, EUROfusion Programme Management Unit, Culham Science Centre, Abingdon, Oxon, OX14 3DB, UK or e-mail Publications.Officer@euro-fusion.org

Enquiries about Copyright and reproduction should be addressed to the Publications Officer, EUROfusion Programme Management Unit, Culham Science Centre, Abingdon, Oxon, OX14 3DB, UK or e-mail Publications.Officer@euro-fusion.org

The contents of this preprint and all other EUROfusion Preprints, Reports and Conference Papers are available to view online free at http://www.euro-fusionscipub.org. This site has full search facilities and e-mail alert options. In the JET specific papers the diagrams contained within the PDFs on this site are hyperlinked

# The universality of point defect structure in body-centred cubic metals

Pui-Wai Ma* and S. L. Dudarev
*CCFE, UK Atomic Energy Authority, Culham Science Centre, Abingdon, Oxfordshire OX14 3DB, United Kingdom*

Formation and migration energies, elastic dipole and relaxation volume tensors of nano-defects are the parameters that determine the rates of evolution of microstructure under irradiation and the magnitude of macroscopic elastic stresses and strains resulting from the accumulation of defects in materials. To find accurate values of these parameters, we have performed density functional theory simulations of self-interstitial and vacancy defects in all the body-centred cubic metals, including alkaline metals (Li, Na, K, Rb and Cs), alkaline-earth metal (Ba), non-magnetic bcc transition metals (V, Nb, Mo, Ta and W), and magnetic transition metals (Cr and Fe), correcting the computed values for the effect of finite cell size and periodic boundary conditions. The lowest energy structure of a self-interstitial atom defect is universal to all the non-magnetic bcc metals, including metals of Group 1 and 2 of the Periodic Table, and has the $\langle 111 \rangle$ symmetry. The only exceptions are the $\langle 110 \rangle$ self-interstitial defect configuration in Fe, and a $\langle 11\xi \rangle$ configuration in Cr. We have also computed elastic dipole tensors and relaxation volumes of self-interstitial and vacancy defects in all the bcc metals and explored how elastic relaxation parameters evolve along defect migration pathways.

## I. INTRODUCTION

Dislocations and point defects in crystalline materials are created by mechanical deformation or by irradiation, followed by the relaxation of locally distorted atomic configurations[1]. A Frenkel pair is a commonly occurring type of radiation defect, in which an atom is removed from a lattice site and placed elsewhere in the lattice, forming a pair of a vacancy and a self-interstitial atom (SIA). In elasticity theory, the strain field associated with a defect can be described by its elastic dipole tensor[2–7]. Matrix elements of elastic dipole tensor can be derived from atomic scale simulations, where interatomic forces are evaluated using empirical potentials or *ab initio* methods. Using elastic dipole tensors, discrete atomic configurations of defects can be treated as objects of continuum elasticity, enabling simulations of evolution of large ensembles of defects on the time and spatial scales many orders of magnitude larger than those accessible to atomic or electronic structure based methods[8].

The dipole tensor of a defect $P_{ij}$ fully defines its properties within the theory of elasticity[9]. The energy of elastic interaction between a defect and external strain field $\epsilon_{ij}^{ext}$ is

$$E_{int}^{ext} = -P_{ij}\epsilon_{ij}^{ext}, \tag{1}$$

whereas the energy of interaction between any two defects separated by the distance many times their size is

$$E_{int}^{ab} = P_{ij}^{a} P_{kl}^{b} \frac{\partial^2}{\partial x_j \partial x_l} G_{ik}(\mathbf{r}), \tag{2}$$

where $P_{ij}^{a}$ and $P_{kl}^{b}$ are the dipole tensors of defects $a$ and $b$, $\mathbf{r}$ is the relative position vector of the defects, and $G_{ik}$ is the elastic Green function. $G_{ik}$ can be evaluated numerically for an arbitrary elastically anisotropic material[10] from the matrix elements of the stiffness tensor. Using equation (2), the energy of elastic interaction can be computed for any configuration of defects, which otherwise is difficult to treat using atomistic or electronic structure based methods due to the limitations imposed by the simulation cell size.

Domain and Becquart[11] computed the dipole tensor of a vacancy (using an *ab initio* approach) and a SIA (using empirical potentials) in iron using the Kanzaki force formalism. Varvenne and Clouet[6] showed how to evaluate the dipole tensor of a defect from macro-stresses in a simulation cell, and investigated the numerical convergence of calculations as a function of cell size. Treating point defects in zirconium, they compared convergence of the two methods and showed that the Kanzaki force and macro-stress approaches produced similar results in the limit where simulation cells were sufficiently large.

Sivak *et al.*[12] investigated elastic interactions between point defects and dislocations in iron, computing them using molecular statics and linear elasticity. Matrix elements of dipole tensors of defects were derived from atomistic calculations, where interaction between the atoms was described by empirical interatomic potentials. They found that the elasticity approximation described the energy of interaction fairly well if a defect and a dislocation line were separated by a distance just a little over three lattice constants, in agreement with the analysis of dislocation core effects by Boleininger *et al.*[13]. Sivak *et al.*[12] also evaluated the dipole tensors of vacancies and SIA defects in iron at equilibrium and saddle points.

Since the elastic energy of interaction between a defect and external strain field can be readily evaluated using the dipole tensor formalism, elastic interaction effects can be included in coarse-grained models, for example in object kinetic Monte-Carlo (kMC). By performing kMC simulations, Sivak *et al.* estimated the effect of elastic interactions on the diffusion of defects in bcc iron and vanadium[14], and also on the diffusion of hydrogen in bcc iron[15,16].

This brings into focus the question about the structure of a defect in a metal. Paneth[17] suggested that in

an alkaline metal a SIA defect would adopt a $\langle 111 \rangle$ configuration. He evaluated the formation energy of a $\langle 111 \rangle$ crowdion in sodium using a model, where a positive point charge was embedded in a uniform field of negative charge density, and found the formation energy to be close to 0.3 eV. Other researchers later argued that it was the $\langle 110 \rangle$ dumbbell that represented the most stable SIA defect configuration in Fe and Mo[3,18,19].

Different SIA configurations have different mobilities. A $\langle 111 \rangle$ defect structure can easily translate itself through the lattice in the direction parallel to its axis, suggesting that a crowdion should be highly mobile[20]. This explains the high diffusivity of SIAs observed in experiments on resistivity recovery of electron irradiated metals[21–23]. Experimental observations show that in many bcc metals SIA defects still move at temperatures below 6K. High-voltage electron microscope experiments[24] also show that the activation energy for the long-range migration of SIA defects in tungsten is low. On the other hand, a $\langle 110 \rangle$ dumbbell migrates through a sequence of translation and rotational jumps[3,18] and its three-dimensional diffusion is strongly thermally activated.

*Ab initio* density function theory (DFT) calculations have been recently applied to the evaluation of formation and migration energies of defects in bcc metals and to the calculation of relaxation volumes of defects[19,25–33]. In all of the non-magnetic bcc transition metals, the most stable SIA defect structure was found to have the $\langle 111 \rangle$ symmetry[25,26]. Swinburne *et al.*[34] showed that the migration energy of a $\langle 111 \rangle$ dumbbell in tungsten is close to 2 meV, and that the saddle point configuration on a defect migration pathway is a $\langle 111 \rangle$ crowdion. Quantum fluctuations of atomic positions make the $\langle 111 \rangle$ SIA defects extremely mobile at temperatures as low as 1K[34].

The only *ab initio* study of SIA defects in alkaline metals so far was performed by Breier *et al.*[27]. They evaluated the formation energies of $\langle 111 \rangle$, $\langle 110 \rangle$ and $\langle 100 \rangle$ SIA dumbbells in sodium using the local density approximation (LDA). The $\langle 110 \rangle$ dumbbell was found to have the lowest energy, although it was only 0.01eV lower than the energy of the $\langle 111 \rangle$ dumbbell configuration. Calculations in Ref.[27] were performed using a relatively small 55 atom cell. Below, we compare these results with calculations performed using more accurate density functionals and larger simulation cells. We also investigate the structure of defects in all the other bcc metals of the Periodic Table, including alkaline metals.

In iron, the $\langle 110 \rangle$ dumbbell is the most stable SIA configuration[11,25,26]. The three-dimensional translation-rotation migration pathway of the defect[19] explains the relatively high activation temperature for diffusion of SIAs in iron[21,22], which is close to 120K.

The structure of an SIA defect in chromium remains somewhat uncertain. Calculations assuming a non-magnetic (NM) electronic ground state[25,26] or an antiferromagnetic (AFM) state[35,36] showed that the difference between the formation energies of $\langle 111 \rangle$ and $\langle 110 \rangle$ dumbbells was within the margin of error of *ab initio* calculations. Recently, we found[37] that the most stable configuration of a SIA in Cr has the $\langle 11\xi \rangle$ orientation, where $\xi$ varies from 0.355 to 0.405, regardless of magnetic order. This requires further verification, and is a subject of further work.

In this paper, in addition to determining the structure and energies of various defect configurations, we also evaluate their elastic properties needed for the long time and large spatial scale dynamic simulations of microstructure. We start by computing the formation and migration energies of defects, treating interactions with periodic images in the linear elasticity approximation. Then, we evaluate the dipole tensors and relaxation volume tensors of all the defect structures in all the bcc metals, including alkaline metals Li, Na, K, Rb and Cs, alkaline-earth metal Ba, the non-magnetic transition metals V, Nb, Mo, Ta and W, and magnetic transition metals Cr and Fe. Thermal migration of a $\langle 111 \rangle$ SIA defect proceeds through a sequence of $\langle 111 \rangle$ crowdion $\leftrightarrow$ $\langle 111 \rangle$ dumbbell transformations. This involves almost no variation of the elastic dipole tensor. On the other hand, when investigating the migration of a $\langle 110 \rangle$ defect configuration in Fe, we find that it involves some significant variation of the dipole tensor along the migration pathway.

## II. THEORY

We start by briefly reviewing the methodology for computing the formation and migration energies, dipole and relaxation volume tensors, and variation of these quantities along defect migration pathways.

The formation energy of a defect $E^F_{def}$ is

$$E^F_{def} = E_{def}(N_{def}) - \frac{N_{def}}{N_{bulk}} E_{bulk}(N_{bulk}), \qquad (3)$$

where $E_{def}$ is the energy of a simulation cell containing a defect, $E_{bulk}$ is the energy of a reference defect-free cell, and $N_{def}$ and $N_{bulk}$ are the numbers of atoms in the respective cells.

Equation (3) leaves open the question about whether the simulation cell should be fully relaxed, or the relaxation of ion positions should be performed in a constrained manner, leaving the boundaries of the cell fixed. The subtlety of equation (3) is also associated with the fact that it implicitly assumes the limit $N_{def}, N_{bulk} \to \infty$, which is never achieved in a practical simulation. To circumvent the need to treat surface termination effects, simulations of defects are normally performed using periodic boundary conditions. This is equivalent to evaluating the energy associated with embedding an infinite number of defects in an infinite medium. Naturally, to relate the formation energy defined by equation (3) to a calculation performed using periodic boundary conditions, it is necessary to subtract from the result of an *ab initio* calculation the energy of interaction between a

defect and all its periodic images, and estimate the contribution associated with lattice deformation generated by the infinite number of images of the defect.

An alternative approach is to relax the orientation and positions of the boundaries of the cell in order to arrive at a stress-free state of the material. Varvenne *et al.*[5,6] noted that the stress-free approach exhibited better numerical convergence as a function of simulation cell size, and produced lower values of defect formation energies. The relaxation of positions and orientations of boundaries of the simulation cell containing a defect is equivalent to applying homogeneous elastic strain $\boldsymbol{\epsilon}^{app}$. The elastic energy associated with this strain $E^{app}$ contributes to the formation energy of the defect.

The strain tensor $\boldsymbol{\epsilon}^{app}$, associated with the relaxation of boundaries of the simulation cell, satisfies the condition

$$\mathbf{V}^{ref}(\mathbf{I}+\boldsymbol{\epsilon}^{app}) = \mathbf{V}^{def} \tag{4}$$

where $\mathbf{I}$ is an identity matrix, $\mathbf{V}^{ref} = \{\mathbf{L}_1^{ref}, \mathbf{L}_2^{ref}, \mathbf{L}_3^{ref}\}$ is a matrix of translation vectors of the reference cell and $\mathbf{V}^{def} = \{\mathbf{L}_1^{def}, \mathbf{L}_2^{def}, \mathbf{L}_3^{def}\}$ is a matrix of translation vectors of the cell containing a defect. The elastic energy associated with strain $\boldsymbol{\epsilon}^{app}$ is[5]:

$$E^{app} = \frac{V^{ref}}{2} C_{ijkl}\epsilon_{ij}^{app}\epsilon_{kl}^{app} - P_{ij}\epsilon_{ij}^{app}, \tag{5}$$

where $V^{ref}$ is the volume of the simulation cell and $C_{ijkl}$ is the elastic constant tensor. The quadratic term in equation (5) is the elastic energy associated with the deformation of the simulation box, whereas the second term is the energy of interaction between the defect and the applied strain. Since equation (5) is valid in the limit $\|\epsilon^{app}\| \ll 1$, we neglect the difference between the volumes of the reference cell and the cell containing a defect.

Equation (3) for the formation energy of the defect now acquires the form

$$E_{def}^{F} = [E_{def}(N_{def}) - E^{app}] - \frac{N_{def}}{N_{bulk}} E_{bulk}(N_{bulk}) - E_{int} \tag{6}$$

where $E_{int}$ is the energy of elastic interaction between a defect and its periodic images. Since the above consideration applies to any configuration of a defect, equation (6) remains valid everywhere on a defect migration pathway. For example, the migration energy $E_{def}^{M}$ corresponding to the saddle point on a transition pathway can also be evaluated using equation (6).

Values of $E_{int}$ for various defect configurations can be evaluated from the dipole tensor of the defect and anisotropic elastic Green's function of the crystal[4–7]. The energy of elastic interaction between a defect and its periodic images can be written as[7]

$$E_{int} = E_{int}^{total} - E_{corr}, \tag{7}$$

where

$$E_{int}^{total} = \frac{1}{2}\sum_{n\neq 0} P_{ij}P_{kl}\frac{\partial}{\partial x_j}\frac{\partial}{\partial x_l}G_{ik}(\mathbf{R_n}) \tag{8}$$

is a conditionally convergent sum of energies of elastic interaction between a defect and all of its periodic images situated at $\mathbf{R}_n$, and

$$E_{corr} = \frac{1}{2V_{cell}}\int_{V_{cell}} \sum_{n\neq 0} P_{ij}P_{kl}\frac{\partial}{\partial x_j}\frac{\partial}{\partial x_l}G_{ik}(\mathbf{R_n}-\mathbf{r})d^3r \tag{9}$$

is a term that regularizes the strain generated by periodic images and ensures the absolute convergence of summation over $n$.

The dipole tensor of a localized defect can be calculated through macro-stresses developing in a simulation box due to the presence of a defect[5,7]. The calculation is exact if all the non-linear deformations associated with the defect structure are contained entirely within the cell[7], even if the cell size is relatively small. The dipole tensor is computed using the equation[4–7]

$$P_{ij} = V_{cell}(C_{ijkl}\epsilon_{kl}^{app} - \bar{\sigma}_{ij}), \tag{10}$$

where

$$\bar{\sigma}_{ij} = \frac{1}{V_{cell}}\int_{V_{cell}} \sigma_{ij} dV \tag{11}$$

is the average macroscopic stress in the simulation box. The relaxation volume tensor, proportional to the so-called $\lambda$-tensor[2], is defined as

$$\Omega_{ij} = S_{ijkl}P_{kl} \tag{12}$$

where $\mathbf{S} = \mathbf{C}^{-1}$ is the elastic compliance tensor, satisfying the condition $C_{ijkl}S_{klmn} = \frac{1}{2}(\delta_{im}\delta_{jn} + \delta_{in}\delta_{jm})$. The relaxation volume of the defect is given by the trace of tensor $\Omega_{ij}$, namely

$$\Omega_{rel} = Tr\Omega_{ij} = \Omega_{11} + \Omega_{22} + \Omega_{33}. \tag{13}$$

In the next section we summarize results of *ab initio* calculations of energies and elastic properties of defects in all the bcc metals in the Periodic table, including alkaline, alkaline-earth, and transition $3d$, $4d$ and $5d$ metals.

## III. EQUILIBRIUM CONFIGURATIONS OF DEFECTS

The *ab initio* calculations described below were performed using Vienna Ab initio Simulation Package (VASP)[38–41], using supercells containing 4x4x4 bcc unit cells and a 5x5x5 $k$-point mesh. The plane wave energy cutoff for Li was chosen at 1500 eV, for Na and K it at 780 eV, for Rb and Cs at 660 eV, for Ba at 560 eV, and for all the other elements at 450 eV. We used the projector augmented-wave method (PAW) potentials[42,43] and the GGA-PBE[44] exchange-correlation functional. Defects in non-magnetic transition metals were also explored using the AM05[45–47] exchange-correlation functional. There are 3, 7, 9, 9, 9 and 10 valence electrons per atom in Li,

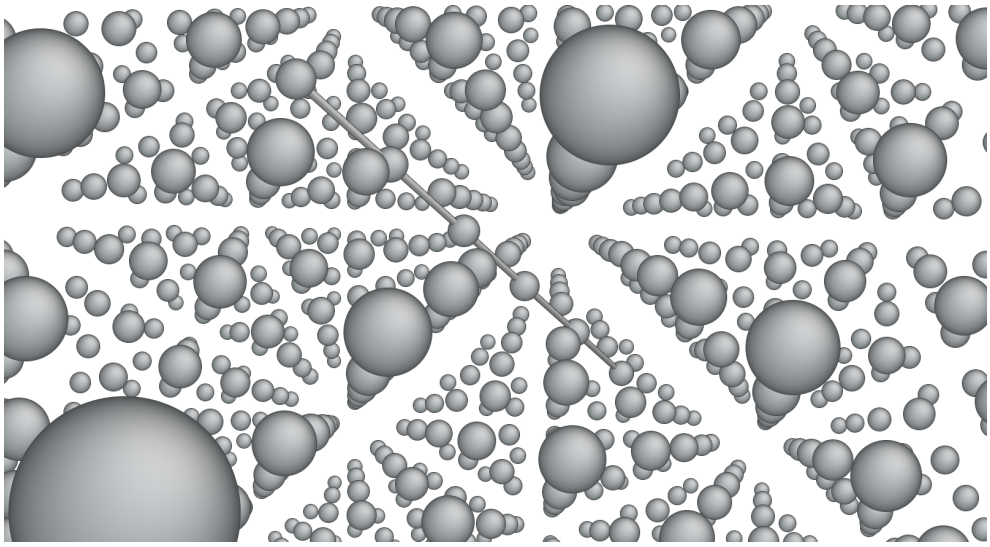

FIG. 1. (Color online) Sketch of the atomic structure of a ⟨111⟩ self-interstitial atom dumbbell defect in bcc lattice.

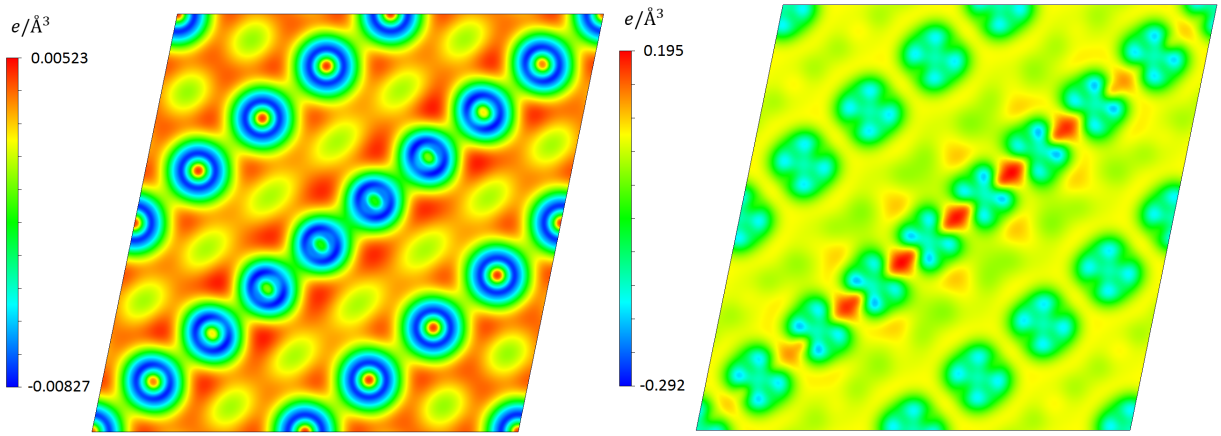


FIG. 2. (Color online) Two-dimensional plots of electron charge density difference in sodium (left) and tungsten (right), computed for a ⟨111⟩ dumbbell SIA defect in the $(\bar{2}11)$ plane. Electron charge density difference equals the fully convergent electron density computed *ab initio* minus the superposition of atomic charge densities.

Na, K, Rb, Cs and Ba, and 11, 12, 14, 11, 12, 11 and 12 valence electrons per atom in V, Cr, Fe, Nb, Mo, Ta and W, respectively.

Calculations of defect structures in Cr and Fe were performed in the collinear magnetic approximation. Otherwise, we assumed the metals to be non-magnetic, in agreement with experimental observations. The ground state of Cr was assumed to be anti-ferromagnetic (AFM). Detailed analysis shows that the true ground electronic state of Cr has the form of a spin density wave (SDW)[48], but within the error margin of *ab initio* calculations the energy of this SDW state is practically indistinguishable from that of the AFM state[49]. All the calculations for Fe were performed assuming a collinear ferromagnetic (FM) electronic ground state[50,51].

The calculations were performed as follows. For each metal, we relaxed a simulation cell containing 128 atoms arranged in a perfect bcc lattice structure, and computed the equilibrium value of the lattice constant. Then, by inserting an extra atom in a cell we formed various SIA configurations, including a ⟨111⟩ dumbbell, ⟨111⟩ crowdion, ⟨110⟩ dumbbell, tetrahedral interstitial, ⟨100⟩ dumbbell, and octahedral interstitial, or created a vacancy by removing an atom from a lattice site. Ion positions were relaxed without altering the shape and volume of the simulation cell. The convergence condition was defined by the maximum force acting on any atom in the cell, which was set to be less than 0.01 eV/Å.

To evaluate the relaxation volume tensor, we need to know the elements of the compliance tensor $S_{klmn}$, which can be computed from the tensor of elastic constants $C_{ijkl}$. Elastic constant tensors for various metals were computed using the Le Page and Saxe method[52], using a 2 atoms simulation cell and a 30x30x30 $k$-point mesh.

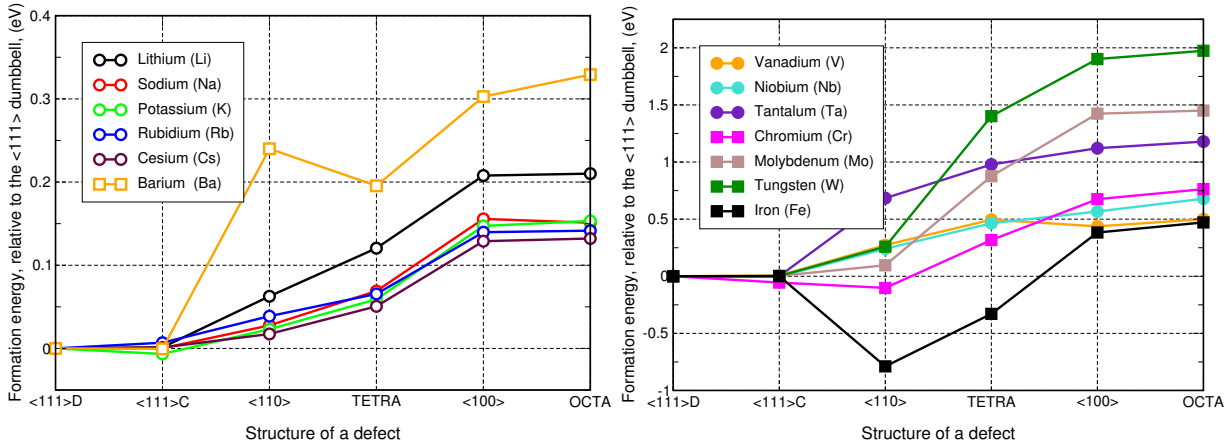


FIG. 3. (Color online) Formation energies of various self-interstitial atom (SIA) defect configurations in bcc metals. Formation energies are shown using the formation energy of a ⟨111⟩ dumbbell as a reference value for a given metal.

The atomic volume $\Omega_0$ and the value of the equilibrium lattice constant $a_0$ for each metals were taken from a 128 atom cell perfect lattice calculation. The results are summarized in Table I together with experimental data. The calculated values are generally in agreement with experimental data.

We start by verifying the validity of Eq. 6. Using tungsten as an example, we compute $E_{def}$, $E^{app}$, $E_{int}$, and $E^F_{def}$ for a vacancy and various SIA configurations, using relaxed and unrelaxed simulation cells. Tables II and III show that the computed formation energies of point defects $E^F_{def}$ are compatible with each other. The values of $E_{def}$ can vary significantly if the simulation cell is relaxed arbitrarily without considering elastic corrections. The resulting values of defect formation energies $E^F_{def}$ in tungsten, computed using the relaxed and unrelaxed cell approaches, differ by less than 0.1%.

In Tables IV and V, we summarize the computed formation energies of all the point defects in all the bcc metals. With the exception of magnetic transition metals (Cr and Fe), self-interstitial defects in all the bcc metals universally adopt the ⟨111⟩ dumbbell or crowdion lowest energy configuration. A sketch of this universal ⟨111⟩-type self-interstitial defect structure is shown in Fig. 1.

Formation energies of defects given in Tables IV and V show that the difference between energies of ⟨111⟩ dumbbell and crowdion configurations is in the meV range. A similar pattern of stability of defects was found by Nguyen-Manh *et al.*[25] and Derlet *et al.*[26] in non-magnetic transition metals. Our results for these metals agree with earlier calculations, and this is also confirmed by additional calculations performed using the AM05 functional. Furthermore, we find that the trend exhibited by configurations of defects in bcc alkaline and alkaline-earth metals remains the same as in non-magnetic bcc transition metals. The fact that the structure of a defect depends only on the structure of the surrounding crystal lattice and does not depend, for example, on the directionality of the type of bonding between the atoms in a metal is unexpected, and is one of the key findings of this work.

Fig. 2 show a two-dimensional plot of electron charge density difference in sodium and tungsten, computed for a ⟨111⟩ dumbbell SIA defect in the $(\bar{2}11)$ plane. Electron charge density difference equals the fully convergent electron density computed *ab initio* minus the superposition of atomic charge densities. The two dimensional plots shows that bonding in the two metals clearly has different character, and is mediated by $s$ and $d$ electrons, respectively. Still, the lowest-energy structure of the defect itself is the same in both metals. A defect forms an area of strong local deformation extended in the ⟨111⟩ direction. The distance between the atoms in the ⟨111⟩ strings is the shortest in bcc lattice. It appears that in Na the defect structure is stabilized by the maxima of electron densities between atoms in the ⟨111⟩ strings, which is similar to bonds in molecules[53]. In tungsten, the charge density difference shows no evidence of the part played by directional $d$-bonding, and the electronic phenomenon responsible for the anomalously high stability of the ⟨111⟩ defect structure appears elusive.

Fig. 3 illustrates, in a graphical form, the data listed in Table IV. In the Figure, all the values are shown relative to the ⟨111⟩ dumbbell formation energy. Figure 3 shows that in all the non-magnetic bcc metals, an SIA defect adopts either a ⟨111⟩ dumbbell or a ⟨111⟩ crowdion configuration as the lowest energy state. Swinburne *et al.*[34], using DFT and the nudge elastic band method, showed that a ⟨111⟩ SIA in tungsten migrates through a sequence of dumbbell↔crowdion↔dumbbell steps with a barrier that is as low as 2 meV. Given such a low migration barrier, it is hardly surprising that quantum fluctuations of atomic positions are able to assist the movement of an SIA through the lattice at very low temperatures[24]. The data given in Table IV explain why in many bcc metals, SIA defects are able to migrate at temperatures lower than 6K, in agreement with resistivity recovery experiments[21].

Magnetic transition metals Cr and Fe are the excep-

tions. In Fe, a ⟨110⟩ dumbbell is the most stable configuration of an SIA defect[19,25,26]. Fu *et al.*[19] showed that this explains the origin of the relatively high temperature of stage I of resistivity recovery in electron irradiated iron, which is close to 120K[21]. For a long time, the structure of defects in Cr remained uncertain. We have found[37] that the most stable SIA configuration in Cr is a $\langle 11\xi \rangle$ dumbbell, where $\xi = 0.355$ for the AFM state and $\xi = 0.405$ for the NM state. Calculations suggest that the defect migration pathway in Cr follows a translation-rotation pattern, changing from a $\langle 11\xi \rangle$ to an adjacent $\langle \xi 11 \rangle$ dumbbell configuration[37].

The elements of dipole tensors $P_{ij}$ and relaxation volume tensors $\Omega_{ij}$ for all the defects in all the bcc metals are given in Tables VI to XXIV. We have also determined the eigenvalues $\Omega^{(i)}$ of relaxation volume tensors, and relaxation volumes of defects $\Omega_{rel}$. The eigenvectors of $\Omega_{ij}$ are given in Table XXV. Using these parameters, one can evaluate the strength of elastic interaction between various points defects, and between a point defect and any strain field in a material. The quantities given in Tables VI - XXV relate parameters of defects, derived from simulations performed on the electronic scale, to continuum elasticity. In general, it is necessary to define three parameters, namely the eigenvalues of tensors $P_{ij}$ or $\Omega_{ij}$, to fully characterize the elastic field of a point defect. The eigenvectors reflect the symmetry of a particular configuration of a defect. They remain the same for the same defect configuration, whereas the eigenvalues vary from one material to another.

Defects in non-magnetic transition metals were studied using the PBE and AM05 functionals, which give slightly different predictions. If we use the relaxation volume $\Omega_{rel}$ of a defect as a criterion to compare the difference between results obtained using the PBE and AM05 functionals then, with the exception of vanadium, the difference is smaller than 5%. This 5% error is in fact compatible with the error margin of the linear elasticity approximation associated with the relative size of the core of the defect and the simulation cell[7]. Using semi-empirical potentials and molecular statics calculations, we found that obtaining a converged value of the dipole tensor requires using a cell containing at least a few thousand atoms[7]. For vanadium, the difference between the values computed using the two functionals is greater. At this point, it is difficult to establish what exchange-correlation functional is more applicable to the quantitative prediction of elastic properties of defects in vanadium.

We have also computed elastic parameters of defects in tungsten, using zero stress simulations. Tables XX and XXI show values computed using fixed and relaxed boundary conditions. The values computed by two different methods are comparable, and the difference between them is due to the fact that a finite value of applied strain was used when computing the elastic correction, whereas linear elasticity is valid only in the limit of infinitesimally small strain.

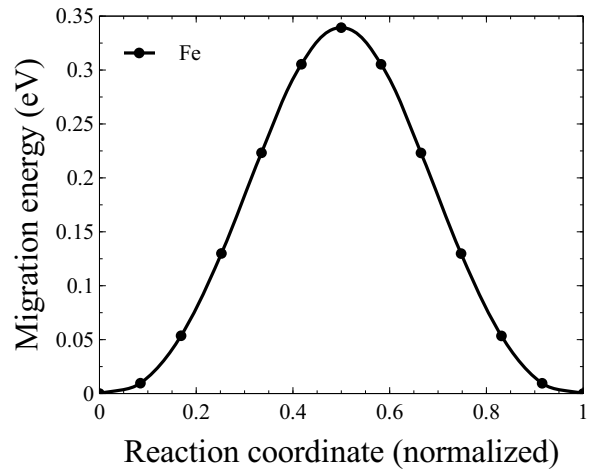


FIG. 4. (Color online) Variation of energy along the pathway of migration of a ⟨110⟩ dumbbell in Fe.

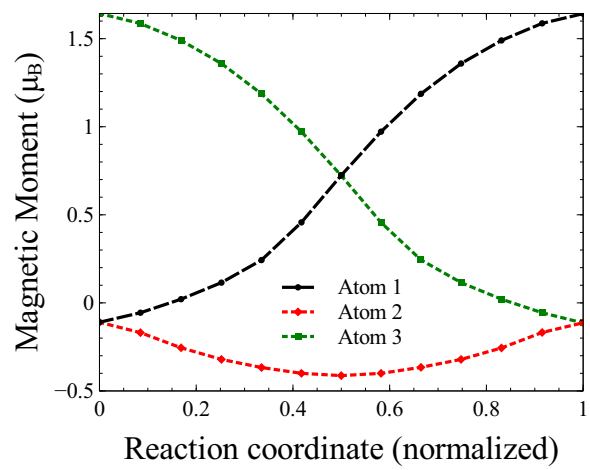


FIG. 5. (Color online) Magnetic moments of the three atoms undergoing the greatest displacement during the migration of a ⟨110⟩ dumbbell in Fe. Atoms 1 and 2 are the two atoms that are initially at the centre of the SIA configuration, whereas atoms 2 and 3 form of the centre of the defect at its final position.

## IV. MIGRATION OF A SELF-INTERSTITIAL ATOM DEFECT IN IRON AND CHROMIUM

The translation-rotation migration step of a ⟨110⟩ dumbbell in Fe was examined using nudge elastic band (NEB) method calculations[54,55]. Eleven images were used to represent the trajectory linking the initial and final equilibrium positions of the defect. Fig. 4 shows how the energy of the defect varies when a ⟨110⟩ dumbbell migrates along its transition pathway. All the data points are corrected according to Eq. 6. The saddle point energy of 0.34 eV for migration of an SIA defect in Fe agrees with the value computed by Fu *et al.*[19].

Since Fe is ferromagnetic, it is interesting to study

its magnetic configuration. During the migration, the magnetic configuration changes according to the position of the core of the ⟨110⟩ dumbbell configuration. The changes of magnetic moments are shown in Fig. 5 and 6. At the core of the ⟨110⟩ dumbbell, the magnetic moments of the two atoms are ordered antiferromagnetically with respect to the lattice. When the core migrates, one of the two core atoms replaces an adjacent atom. The magnetic configuration remains the same at the equilibrium positions whereas at the saddle point, we observe that the magnetic moment of only one atom is antiferromagnetically ordered with respect to the surrounding lattice. Given that migration of the defect can occur at a relatively low temperature, well below the Curie temperature of iron, it would be interesting to explore whether the magnetic dynamics of atomic moments has an effect on the migration pathway.

Variation of the elements of elastic dipole tensor of a ⟨110⟩ dumbbell in Fe along the defect migration pathway is illustrated in Fig. 7. The evolution of the relaxation volume tensor along the same pathway is illustrated in Fig. 8. The figures show that elements $P_{11}$ and $P_{33}$ change due to the change of orientation of the ⟨110⟩ defect from its initial position in the x-y plane to its final position in the y-z plane. A similar variation is observed for the off-diagonal elements of tensor $P_{ij}$, and for the elements of the relaxation volume tensor.

The above results pose an interesting question, related to the timescale of the process of migration, and the validity of elastic approximation for the treatment of defect configurations along the migration pathway. The static elastic approximation remains valid if the process of migration is slow in comparison with the time required for sound waves to propagate to the object with which a migrating defect interacts. At large distances between any two interacting defects one is expected to observe delayed elastic interaction, mediated by sound waves propagating through the material slower than the time required for a defect to complete its translation-rotation jump.

## V. CONCLUSIONS

In this study, we have investigated formation and migration energies, elastic dipole and relaxation volume tensors of self-interstitial and vacancy defects in all the bcc metals in the Periodic Table. In all these metals, including metals of Group 1 and 2, the lowest energy structure of a self-interstitial atom defect is universal and has the ⟨111⟩ symmetry. In ferromagnetic Fe, a SIA defects adopt the ⟨110⟩ dumbbell configurations. We have also computed elastic dipole tensors and relaxation volumes of self-interstitial and vacancy defects in all the bcc metals and explored how elastic relaxation parameters evolve along the defect migration pathways.

| | $C_{11}$ (GPa) | $C_{12}$ (GPa) | $C_{44}$ (GPa) | $\Omega_0$ (Å$^3$) | $a_0$ (Å) |
|---|---|---|---|---|---|
| Li | 18.14 | 11.85 | 11.43 | 20.24 | 3.434 |
| | *14.85*[a] | *12.53*[a] | *10.80*[a] | *21.27*[b] | *3.491*[b] |
| Na | 9.34 | 7.44 | 5.96 | 36.94 | 4.196 |
| | *8.57*[c] | *7.11*[c] | *5.87*[c] | *37.71*[b] | *4.225*[b] |
| K | 3.91 | 3.44 | 2.70 | 73.63 | 5.281 |
| | *4.17*[d] | *3.41*[d] | *2.86*[d] | *71.32*[b] | *5.225*[b] |
| Rb | 3.07 | 2.65 | 1.99 | 90.92 | 5.665 |
| | *3.25*[e] | *2.73*[e] | *1.98*[e] | *87.10*[b] | *5.585*[b] |
| Cs | 2.16 | 1.85 | 1.38 | 116.74 | 6.158 |
| | *2.47*[f] | *2.06*[f] | *1.48*[f] | *110.45*[b] | *6.045*[b] |
| Ba | 12.06 | 7.31 | 10.39 | 63.55 | 5.028 |
| | *13.0*[g] | *7.6*[g] | *11.8*[g] | *63.25*[b] | *5.02*[b] |
| V | 279.59 | 142.02 | 26.72 | 13.40 | 2.993 |
| | **308.53** | **147.96** | **31.31** | **12.91** | **2.955** |
| | *227.9*[h] | *118.7*[h] | *42.6*[h] | *13.91*[b] | *3.03*[b] |
| Nb | 248.76 | 135.24 | 19.46 | 18.33 | 3.322 |
| | **273.54** | **143.06** | **23.62** | **17.68** | **3.282** |
| | *246.6*[h] | *133.2*[h] | *28.1*[h] | *17.97*[b] | *3.30*[b] |
| Mo | 469.07 | 157.72 | 99.71 | 15.77 | 3.160 |
| | **505.43** | **175.26** | **108.04** | **15.24** | **3.124** |
| | *464.7*[h] | *161.5*[h] | *108.9*[h] | *15.63*[b] | *3.15*[b] |
| Ta | 266.28 | 161.36 | 76.75 | 18.29 | 3.320 |
| | **293.44** | **168.18** | **82.08** | **17.62** | **3.278** |
| | *266.0*[h] | *161.2*[h] | *82.4*[h] | *17.97*[b] | *3.30*[b] |
| W | 518.26 | 199.77 | 142.09 | 16.14 | 3.184 |
| | **569.73** | **211.52** | **157.16** | **15.61** | **3.149** |
| | *522.4*[h] | *204.4*[h] | *160.6*[h] | *15.78*[b] | *3.16*[b] |
| Cr | 448.12 | 62.03 | 102.13 | 11.72 | 2.862 |
| | *394.1*[i] | *88.5*[i] | *103.75*[i] | *11.94*[b] | *2.88*[b] |
| Fe | 289.34 | 152.34 | 107.43 | 11.34 | 2.831 |
| | *243.1*[j] | *138.1*[j] | *121.9*[j] | *11.82*[b] | *2.87*[b] |

[a]Ref.[56], [b]Ref.[57], [c]Ref.[58], [d]Ref.[59], [e]Ref.[60], [f]Ref.[61], [g]Ref.[62], [h]Ref.[63], [i]Ref.[64], [j]Ref.[65].

TABLE I. Elastic constants (in GPa units) calculated using the Le Page and Saxe[52] method for a 2-atom cell, 30x30x30 k-points, and GGA-PBE exchange-correlation functional. Atomic volumes (Å$^3$) and lattice constants (Å) were taken from relaxed 128 atoms perfect lattice simulations. Numbers in italic are experimental values. Numbers in bold were computed using the AM05 exchange-correlation functional.

## ACKNOWLEDGMENTS

This work has been carried out within the framework of the EUROfusion Consortium and has received funding from the Euratom research and training programme 2014-2018 under grant agreement No 633053 and from the RCUK Energy Programme [grant number EP/P012450/1]. To obtain further information on the data and models underlying this paper please contact

| W | $E_{def}$ | $E^{app}$ | $E_{int}$ | $E^F_{def}$ |
|---|---|---|---|---|
| ⟨111⟩d | -1661.14271 | 0.000 | -0.0618 | 10.559 |
| ⟨111⟩c | -1661.14079 | 0.000 | -0.0621 | 10.561 |
| ⟨110⟩d | -1660.82332 | 0.000 | -0.0013 | 10.818 |
| Tetra | -1659.65294 | 0.000 | 0.0262 | 11.960 |
| ⟨100⟩d | -1659.14955 | 0.000 | 0.0289 | 12.461 |
| Octa | -1659.07430 | 0.000 | 0.0323 | 12.533 |
| Vac | -1642.49111 | 0.000 | 0.0006 | 3.231 |

TABLE II. The total energy $E_{def}$ of a simulation cell containing a defect, the applied strain energy $E^{app}$, the elastic interaction energy $E_{int}$, and the formation energy $E^F_{def}$ of a defect in W, where the total energy per atom in a perfect lattice is $E_{bulk} = -1658.68112$eV. The values are computed using 4x4x4 unit cells. The shape and the volume of simulation cells containing defects are the same as those of the perfect lattice cell, with no relaxation of boundary conditions. All the values are given in eV units.

| W | $E_{def}$ | $E^{app}$ | $E_{int}$ | $E^F_{def}$ |
|---|---|---|---|---|
| ⟨111⟩d | -1661.63185 | -0.482 | -0.0589 | 10.549 |
| ⟨111⟩c | -1661.63029 | -0.483 | -0.0594 | 10.552 |
| ⟨110⟩d | -1661.22696 | -0.399 | -0.0021 | 10.814 |
| Tetra | -1660.04923 | -0.394 | 0.0282 | 11.956 |
| ⟨100⟩d | -1659.57943 | -0.427 | 0.0293 | 12.458 |
| Octa | -1659.50929 | -0.432 | 0.0335 | 12.529 |
| Vac | -1642.50287 | -0.013 | 0.0006 | 3.232 |

TABLE III. The total energy $E_{def}$ of a simulation cell containing a defect, the applied strain energy $E^{app}$, the elastic interaction energy $E_{int}$, and the formation energy $E^F_{def}$ of a defect in W, where the total energy per atom in a perfect lattice is $E_{bulk} = -1658.68112$eV. The values are computed using 4x4x4 unit cells. The shape and the volume of simulation cells containing defects are relaxed to the stress-free condition. All the values are given in eV units.

PublicationsManager@ukaea.uk. The views and opinions expressed herein do not necessarily reflect those of the European Commission. SLD acknowledges support from the Centre for Non-Linear Studies at LANL. We also acknowledge EUROFusion for the provision of access to Marconi supercomputer facility at CINECA in Italy.

* Leo.Ma@ukaea.uk

[1] W. Cai and W. D. Nix, *Imperfections in Crystalline Solids*, (Cambridge University Press, Cambridge, England, UK, 2016)

[2] P. H. Dederichs, C. Lehmann, H. R. Schober, A. Scholz and R. Zeller, *Lattice theory of point defects*, J. Nucl. Mater. **69**, 176 (1978)

[3] W. Schilling, *Self-interstitial atoms in metals*, J. Nucl. Mater. **69**, 465 (1978)

[4] E. Clouet, S. Garruchet, H. Nguyen, M. Perez, C. S. Becquart, *Dislocation interaction with C in α-Fe: A comparison between atomic simulations and elasticity theory*, Acta Mater. **56**, 3450 (2008)

[5] C. Varvenne, F. Bruneval, M.-C. Marinica and E. Clouet, *Point defect modeling in materials: Coupling ab initio and elasticity approaches*, Phys. Rev. B **88**, 134102 (2013)

[6] C. Varvenne and E. Clouet, *Elastic dipoles of point defects from atomistic simulations*, Phys. Rev. B **96**, 224103 (2017)

[7] S. L. Dudarev and P.-W. Ma, *Elastic fields, dipole tensors, and interaction between self-interstitial atom defects in bcc transition metals*, Phys. Rev. Mater. **2**, 033602 (2018)

[8] S. L. Dudarev, M. R. Gilbert, K. Arakawa, H. Mori, Z. Yao, M. L. Jenkins, and P. M. Derlet, *Langevin model for real-time Brownian dynamics of interacting nanodefects in irradiated metals*, Phys. Rev. B**81**, 224107 (2010)

[9] G. Leibfried and N. Breuer, *Point Defects in Metals* (Springer, Berlin, 1978), p. 161

[10] D. M. Barnett, *The precise evaluation of derivatives of the anisotropic elastic Green's functions*, Phys. Stat. Sol. (b) **49**, 741 (1972)

[11] C. Domain and C. S. Becquart, *Ab initio calculations of defects in Fe and dilute Fe-Cu alloys*, Phys. Rev. B **65**, 024103 (2001)

[12] A. B. Sivak, V. A. Romanov and V. M. Chernov, *Diffusion of self-point defects in body-centered cubic iron crystal containing dislocations*, Crystallography Reports **55**, 97 (2010)

[13] M. Boleininger, T. D. Swinburne, and S. L. Dudarev, *Atomistic-to-continuum description of edge dislocation core: Unification of the Peierls-Nabarro model with linear elasticity*, Phys. Rev. Materials **2**, 083803 (2018)

[14] A. B. Sivak, V. M. Chernov, V. A. Romanov and P. A. Sivak, *Kinetic Monte-Carlo simulation of self-point defect diffusion in dislocation elastic fields in bcc iron and vanadium*, J. Nucl. Mater. **417**, 1067 (2011)

[15] A. B. Sivak, P. A. Sivak, V. A. Romanov and V. M. Chernov, *Energetic, crystallographic and diffusion characteristics of hydrogen isotopes in iron*, J. Nucl. Mater. **461**, 308 (2015)

[16] A. B. Sivak, P. A. Sivak, V. A. Romanov and V. M. Chernov, *Hydrogen diffusion in the elastic fields of dislocations in iron*, Phys. Atomic Nuclei **79**, 1199 (2016)

[17] H. R. Paneth, *The Mechanism of Self-Diffusion in Alkali Metals*, Phys. Rev., **80**, 708 (1950)

[18] F. W. Young, Jr., *Interstitial mobility and interactions*, J. Nucl. Mater **69**, 310 (1978)

[19] C.-C. Fu, F. Willaime and P. Ordejón, *Stability and Mobility of Mono- and Di-Interstitials in α-Fe*, Phys. Rev. Lett. **92**, 175503 (2004)

[20] A. Seeger, *Diffusion and Thermal Conversion of Crowdions*, Phys. Status Solidi **38**, 235 (1970)

| PBE | Li | Na | K | Rb | Cs | Ba | V | Nb | Mo | Ta | W | Cr | Fe |
|---|---|---|---|---|---|---|---|---|---|---|---|---|---|
| ⟨111⟩d | 0.5810 | 0.5211 | 0.4686 | 0.4340 | 0.4366 | 1.5349 | 2.5148 | 4.1189 | 7.6533 | 4.9335 | 10.5587 | 6.6839 | 5.2051 |
| ⟨111⟩c | 0.5823 | 0.5213 | 0.4619 | 0.4409 | 0.4377 | 1.5344 | 2.5207 | 4.1172 | 7.6567 | 4.9347 | 10.5609 | 6.6286 | 5.2063 |
| ⟨110⟩d | 0.6437 | 0.5488 | 0.4917 | 0.4728 | 0.4540 | 1.7749 | 2.7880 | 4.3594 | 7.7494 | 5.6173 | 10.8176 | 6.5818 | 4.4161 |
| Tetra | 0.7015 | 0.5901 | 0.5277 | 0.4995 | 0.4872 | 1.7304 | 3.0102 | 4.5828 | 8.5297 | 5.9121 | 11.9605 | 7.0011 | 4.8759 |
| ⟨100⟩d | 0.7888 | 0.6768 | 0.6158 | 0.5737 | 0.5655 | 1.8376 | 2.9518 | 4.6859 | 9.0771 | 6.0548 | 12.4611 | 7.3592 | 5.5884 |
| Octa | 0.7911 | 0.6722 | 0.6219 | 0.5756 | 0.5687 | 1.8640 | 3.0143 | 4.7980 | 9.1041 | 6.1129 | 12.5330 | 7.4468 | 5.6762 |
| Vac | 0.4887 | 0.3415 | 0.3053 | 0.2694 | 0.2552 | 1.0200 | 2.0422 | 2.6589 | 2.7955 | 2.8759 | 3.2310 | 3.0093 | 2.1914 |
| ⟨11ξ⟩d | | | | | | | | | | | | 6.4259 | |

TABLE IV. Formation energies $E^F$ (in eV units) of various self-interstitial atom configurations and a vacancy in bcc metals, computed using the GGA-PBE functional. In chromium, a $\langle 11\xi \rangle$ ($\xi \approx 0.355$) dumbbell is the most stable SIA configuration.

| AM05 | V | Nb | Mo | Ta | W |
|---|---|---|---|---|---|
| ⟨111⟩d | 2.9924 | 4.4250 | 8.0426 | 5.2458 | 11.0760 |
| ⟨111⟩c | 2.9992 | 4.4235 | 8.0458 | 5.2475 | 11.0782 |
| ⟨110⟩d | 3.2487 | 4.6703 | 8.1605 | 5.8846 | 11.3546 |
| Tetra | 3.5096 | 4.9259 | 8.9762 | 6.2245 | 12.5383 |
| ⟨100⟩d | 3.4737 | 5.0898 | 9.5881 | 6.4261 | 13.1124 |
| Octa | 3.5408 | 5.2053 | 9.6191 | 6.4957 | 13.1906 |
| Vac | 2.6221 | 2.9575 | 3.1149 | 3.1846 | 3.6280 |

TABLE V. Formation energies $E^F$ (in eV units) of various self-interstitial atom configurations and a vacancy in bcc non-magnetic transition metals, computed using the AM05 functional.


[21] P. Ehrhart, P. Jung, H. Schultz, and H. Ullmaier, *Atomic Defects in Metals* edited by H. Ullmaier (Springer-Verlag, Berlin, 1991), Vol. 25.

[22] H. Schultz, *Defect parameters of b.c.c. metals: group-specific trends*, Mater. Sci. Eng.: A **141**, 149 (1991).

[23] F. Dausinger and H. Schultz, *Long-Range Migration of Self-Interstitial Atoms in Tungsten*, Phys. Rev. Lett. **35**, 1773 (1975)

[24] T. Amino, K. Arakawa and H. Mori, *Activation energy for long-range migration of self-interstitial atoms in tungsten obtained by direct measurement of radiation-induced point-defect clusters*, Phil. Mag. Lett. **91**, 86 (2011)

[25] D. Nguyen-Manh, A. P. Horsfield, and S. L. Dudarev, *Self-interstitial atom defects in bcc transition metals: Group-specific trends*, Phys. Rev. B **73**, 020101 (2006)

[26] P. M. Derlet, D. Nguyen-Manh, and S. L. Dudarev, *Multiscale modeling of crowdion and vacancy defects in body-centered-cubic transition metals*, Phys. Rev. B **76**, 054107 (2007)

[27] U. Breier, W. Frank, C. Elsässer, M. Fähnle and A. Seeger, *Properties of monovacancies and self-interstitials in bcc Na: An ab initio pseudopotential study*, Phys. Rev. B **50**, 5928 (1994)

[28] R. Benedek, L. H. Yang, C. Woodward and B. I. Min, *Formation energy and lattice relaxation for point defects in Li and Al*, Phys. Rev. B **45**, 2607 (1992)

[29] R. Pawellek, M. Fähnlet, C. Elsässer, K.-M. Ho and C.-T. Chan, *First-principles calculation of the relaxation around a vacancy and the vacancy formation energy in BCC Li*, J. Phys.: Condens. Matter **3**, 2451 (1991)

[30] W. Frank, U. Breier, C. Elsässer and M. Fähnle, *Properties of monovacancies and self-interstitials in bcc Li: An ab initi pseudopotential study*, Phys. Rev. B **48**, 7676 (1993)

[31] W. Frank, U. Breier, C. Elsässer and M. Fähnle, *First-Principles Calculations of Absolute Concentrations and Self-Diffusion Constants of Vacancies in Lithium*, Phys. Rev. Lett. **77**, 518 (1996)

[32] V. Schott, M. Fähnle and P. A. Madden, *Theory of self-diffusion in alkali metals: I. Results for monovacancies in Li, Na, and K*, J. Phys.: Condens. Matter **12**, 1171 (2000)

[33] U. Breier, V. Schott and M. Fähnle, *Ab initio calculation of formation and migration volumes for vacancies in Li and Na*, Phys. Rev. B **55**, 5772 (1997)

[34] T. D. Swinburne, P.-W. Ma and S. L. Dudarev, *Low temperature diffusivity of self-interstitial defects in tungsten*, New J. Phys **19**, 073024 (2017)

[35] P. Olsson, C. Domain, J. Wallenius, *Ab initio study of Cr interactions with point defects in bcc Fe*, Phys. Rev. B, **75**, 014110, 2007

[36] P. Olsson, *Ab initio study of interstitial migration in FeCr alloys*, J. Nucl. Mater. **386**, 86 (2009)

[37] P.-W. Ma and S. L. Dudarev (2018) in preparation

[38] G. Kresse and J. Hafner, *Ab initio molecular dynamics for liquid metals*, Phys. Rev. B **47**, 558 (1993).

[39] G. Kresse and J. Hafner, *Ab initio molecular-dynamics simulation of the liquid-metal-amorphous-semiconductor transition in germanium*, Phys. Rev. B **49**, 14251 (1994).

[40] G. Kresse and J. Furthmüller, *Efficiency of ab-initio total energy calculations for metals and semiconductors using a plane-wave basis set*, Comput. Mat. Sci., **6**, 15 (1996).

[41] G. Kresse and J. Furthmüller, *Efficient iterative schemes for ab initio total-energy calculations using a plane-wave basis set*, Phys. Rev. B **54**, 11169 (1996).

[42] P.E. Blöchl, *Projector augmented-wave method*, Phys. Rev. B 50, 17953 (1994).

[43] G. Kresse, and D. Joubert, *From ultrasoft pseudopotentials to the projector augmented-wave method*, Phys. Rev. B **59**, 1758 (1999).

[44] J. P. Perdew, K. Burke, and M. Ernzerhof, *Generalized Gradient Approximation Made Simple*, Phys. Rev. Lett. **77**, 3865 (1996). Phys. Rev. Lett. 78, 1396 (1997).

[45] R. Armiento and A. E. Mattsson, *Functional designed to include surface effects in self-consistent density functional theory*, Phys. Rev. B **72**, 085108 (2005).

| Li | $P_{11}$ | $P_{22}$ | $P_{33}$ | $P_{12}$ | $P_{23}$ | $P_{31}$ | $\Omega_{11}$ | $\Omega_{22}$ | $\Omega_{33}$ | $\Omega_{12}$ | $\Omega_{23}$ | $\Omega_{31}$ | $\Omega^{(1)}$ | $\Omega^{(2)}$ | $\Omega^{(3)}$ | $\Omega_{rel}$ |
|---|---|---|---|---|---|---|---|---|---|---|---|---|---|---|---|---|
| ⟨111⟩d | 2.071 | 2.071 | 2.071 | 0.796 | 0.796 | 0.796 | 7.930 | 7.930 | 7.930 | 5.577 | 5.577 | 5.577 | 2.353 | 2.353 | 19.084 | 1.175 |
| ⟨111⟩c | 2.063 | 2.063 | 2.063 | 0.761 | 0.761 | 0.761 | 7.899 | 7.899 | 7.899 | 5.334 | 5.334 | 5.334 | 2.566 | 2.566 | 18.567 | 1.171 |
| ⟨110⟩d | 2.109 | 2.188 | 2.188 | 0.000 | 0.727 | 0.000 | 6.936 | 8.947 | 8.947 | 0.000 | 5.096 | 0.000 | 6.936 | 3.851 | 14.043 | 1.227 |
| Tetra | 2.196 | 2.160 | 2.160 | 0.000 | 0.000 | 0.000 | 8.923 | 8.011 | 8.011 | 0.000 | 0.000 | 0.000 | 8.923 | 8.011 | 8.011 | 1.232 |
| ⟨100⟩d | 2.764 | 1.911 | 1.911 | 0.000 | 0.000 | 0.000 | 22.893 | 1.164 | 1.164 | 0.000 | 0.000 | 0.000 | 22.893 | 1.164 | 1.164 | 1.246 |
| Octa | 1.898 | 1.898 | 2.754 | 0.000 | 0.000 | 0.000 | 1.094 | 1.094 | 22.892 | 0.000 | 0.000 | 0.000 | 1.094 | 1.094 | 22.892 | 1.239 |
| Vac | -0.937 | -0.937 | -0.937 | 0.000 | 0.000 | 0.000 | -3.589 | -3.589 | -3.589 | 0.000 | 0.000 | 0.000 | -3.589 | -3.589 | -3.589 | -0.532 |

TABLE VI. Elements of the dipole tensor $P_{ij}$ (in eV units), the relaxation volume tensor $\Omega_{ij}$ (in Å$^3$ units), eigenvalues of the relaxation volume tensor $\Omega^{(i)}$ (in Å$^3$ units), and the relaxation volume of the defect $\Omega_{rel}$ (in atomic volume units $\Omega_0$) computed for Li.

| Na | $P_{11}$ | $P_{22}$ | $P_{33}$ | $P_{12}$ | $P_{23}$ | $P_{31}$ | $\Omega_{11}$ | $\Omega_{22}$ | $\Omega_{33}$ | $\Omega_{12}$ | $\Omega_{23}$ | $\Omega_{31}$ | $\Omega^{(1)}$ | $\Omega^{(2)}$ | $\Omega^{(3)}$ | $\Omega_{rel}$ |
|---|---|---|---|---|---|---|---|---|---|---|---|---|---|---|---|---|
| ⟨111⟩d | 2.468 | 2.468 | 2.468 | 0.889 | 0.889 | 0.889 | 16.326 | 16.326 | 16.326 | 11.946 | 11.946 | 11.946 | 4.380 | 4.380 | 40.219 | 1.326 |
| ⟨111⟩c | 2.461 | 2.461 | 2.461 | 0.882 | 0.882 | 0.882 | 16.279 | 16.279 | 16.279 | 11.851 | 11.851 | 11.851 | 4.428 | 4.428 | 39.982 | 1.322 |
| ⟨110⟩d | 2.575 | 2.478 | 2.478 | 0.000 | 0.738 | 0.000 | 22.068 | 13.871 | 13.871 | 0.000 | 9.924 | 0.000 | 22.068 | 3.947 | 23.794 | 1.348 |
| Tetra | 2.583 | 2.559 | 2.559 | 0.000 | 0.000 | 0.000 | 18.345 | 16.292 | 16.292 | 0.000 | 0.000 | 0.000 | 18.345 | 16.292 | 16.292 | 1.379 |
| ⟨100⟩d | 3.160 | 2.299 | 2.299 | 0.000 | 0.000 | 0.000 | 65.698 | -7.190 | -7.190 | 0.000 | 0.000 | 0.000 | 65.698 | -7.190 | -7.190 | 1.389 |
| Octa | 2.389 | 2.389 | 3.127 | 0.000 | 0.000 | 0.000 | -3.403 | -3.403 | 59.092 | 0.000 | 0.000 | 0.000 | -3.403 | -3.403 | 59.092 | 1.416 |
| Vac | -0.824 | -0.824 | -0.824 | 0.000 | 0.000 | 0.000 | -5.451 | -5.451 | -5.451 | 0.000 | 0.000 | 0.000 | -5.451 | -5.451 | -5.451 | -0.443 |

TABLE VII. Elements of the dipole tensor $P_{ij}$ (in eV units), the relaxation volume tensor $\Omega_{ij}$ (in Å$^3$ units), eigenvalues of the relaxation volume tensor $\Omega^{(i)}$ (in Å$^3$ units), and the relaxation volume of the defect $\Omega_{rel}$ (in atomic volume units $\Omega_0$) computed for Na.

| K | $P_{11}$ | $P_{22}$ | $P_{33}$ | $P_{12}$ | $P_{23}$ | $P_{31}$ | $\Omega_{11}$ | $\Omega_{22}$ | $\Omega_{33}$ | $\Omega_{12}$ | $\Omega_{23}$ | $\Omega_{31}$ | $\Omega^{(1)}$ | $\Omega^{(2)}$ | $\Omega^{(3)}$ | $\Omega_{rel}$ |
|---|---|---|---|---|---|---|---|---|---|---|---|---|---|---|---|---|
| ⟨111⟩d | 2.260 | 2.260 | 2.260 | 0.793 | 0.793 | 0.793 | 33.581 | 33.581 | 33.581 | 23.572 | 23.572 | 23.572 | 10.009 | 10.009 | 80.725 | 1.368 |
| ⟨111⟩c | 2.272 | 2.272 | 2.272 | 0.760 | 0.760 | 0.760 | 33.761 | 33.761 | 33.761 | 22.588 | 22.588 | 22.588 | 11.174 | 11.174 | 78.937 | 1.376 |
| ⟨110⟩d | 2.316 | 2.293 | 2.293 | 0.000 | 0.743 | 0.000 | 39.646 | 31.461 | 31.461 | 0.000 | 22.085 | 0.000 | 39.646 | 9.376 | 53.546 | 1.393 |
| Tetra | 2.347 | 2.356 | 2.356 | 0.000 | 0.000 | 0.000 | 32.914 | 35.995 | 35.995 | 0.000 | 0.000 | 0.000 | 32.914 | 35.995 | 35.995 | 1.425 |
| ⟨100⟩d | 2.875 | 2.144 | 2.144 | 0.000 | 0.000 | 0.000 | 201.895 | -47.715 | -47.715 | 0.000 | 0.000 | 0.000 | 201.895 | -47.715 | -47.715 | 1.446 |
| Octa | 2.167 | 2.167 | 2.846 | 0.000 | 0.000 | 0.000 | -41.774 | -41.774 | 190.251 | 0.000 | 0.000 | 0.000 | -41.774 | -41.774 | 190.251 | 1.449 |
| Vac | -0.656 | -0.656 | -0.656 | 0.000 | 0.000 | 0.000 | -9.744 | -9.744 | -9.744 | 0.000 | 0.000 | 0.000 | -9.744 | -9.744 | -9.744 | -0.397 |

TABLE VIII. Elements of the dipole tensor $P_{ij}$ (in eV units), the relaxation volume tensor $\Omega_{ij}$ (in Å$^3$ units), eigenvalues of the relaxation volume tensor $\Omega^{(i)}$ (in Å$^3$ units), and the relaxation volume of the defect $\Omega_{rel}$ (in atomic volume units $\Omega_0$) computed for K.

| Rb | $P_{11}$ | $P_{22}$ | $P_{33}$ | $P_{12}$ | $P_{23}$ | $P_{31}$ | $\Omega_{11}$ | $\Omega_{22}$ | $\Omega_{33}$ | $\Omega_{12}$ | $\Omega_{23}$ | $\Omega_{31}$ | $\Omega^{(1)}$ | $\Omega^{(2)}$ | $\Omega^{(3)}$ | $\Omega_{rel}$ |
|---|---|---|---|---|---|---|---|---|---|---|---|---|---|---|---|---|
| ⟨111⟩d | 2.232 | 2.232 | 2.232 | 0.774 | 0.774 | 0.774 | 42.696 | 42.696 | 42.696 | 31.146 | 31.146 | 31.146 | 11.550 | 11.550 | 104.987 | 1.409 |
| ⟨111⟩c | 2.235 | 2.235 | 2.235 | 0.782 | 0.782 | 0.782 | 42.745 | 42.745 | 42.745 | 31.448 | 31.448 | 31.448 | 11.297 | 11.297 | 105.641 | 1.410 |
| ⟨110⟩d | 2.244 | 2.274 | 2.274 | 0.000 | 0.794 | 0.000 | 35.517 | 47.187 | 47.187 | 0.000 | 31.965 | 0.000 | 35.517 | 15.222 | 79.151 | 1.429 |
| Tetra | 2.248 | 2.354 | 2.354 | 0.000 | 0.000 | 0.000 | 17.093 | 57.968 | 57.968 | 0.000 | 0.000 | 0.000 | 17.093 | 57.968 | 57.968 | 1.463 |
| ⟨100⟩d | 2.826 | 2.146 | 2.146 | 0.000 | 0.000 | 0.000 | 221.461 | -42.670 | -42.670 | 0.000 | 0.000 | 0.000 | 221.461 | -42.670 | -42.670 | 1.497 |
| Octa | 2.148 | 2.148 | 2.824 | 0.000 | 0.000 | 0.000 | -42.227 | -42.227 | 220.622 | 0.000 | 0.000 | 0.000 | -42.227 | -42.227 | 220.622 | 1.498 |
| Vac | -0.625 | -0.625 | -0.625 | 0.000 | 0.000 | 0.000 | -11.945 | -11.945 | -11.945 | 0.000 | 0.000 | 0.000 | -11.945 | -11.945 | -11.945 | -0.394 |

TABLE IX. Elements of the dipole tensor $P_{ij}$ (in eV units), the relaxation volume tensor $\Omega_{ij}$ (in Å$^3$ units), eigenvalues of the relaxation volume tensor $\Omega^{(i)}$ (in Å$^3$ units), and the relaxation volume of the defect $\Omega_{rel}$ (in atomic volume units $\Omega_0$) computed for Rb.

| Cs | $P_{11}$ | $P_{22}$ | $P_{33}$ | $P_{12}$ | $P_{23}$ | $P_{31}$ | $\Omega_{11}$ | $\Omega_{22}$ | $\Omega_{33}$ | $\Omega_{12}$ | $\Omega_{23}$ | $\Omega_{31}$ | $\Omega^{(1)}$ | $\Omega^{(2)}$ | $\Omega^{(3)}$ | $\Omega_{rel}$ |
|---|---|---|---|---|---|---|---|---|---|---|---|---|---|---|---|---|
| ⟨111⟩d | 2.066 | 2.066 | 2.066 | 0.722 | 0.722 | 0.722 | 56.556 | 56.556 | 56.556 | 41.921 | 41.921 | 41.921 | 14.635 | 14.635 | 140.399 | 1.453 |
| ⟨111⟩c | 2.066 | 2.066 | 2.066 | 0.725 | 0.725 | 0.725 | 56.572 | 56.572 | 56.572 | 42.084 | 42.084 | 42.084 | 14.488 | 14.488 | 140.740 | 1.454 |
| ⟨110⟩d | 2.072 | 2.057 | 2.057 | 0.000 | 0.698 | 0.000 | 61.527 | 53.917 | 53.917 | 0.000 | 40.547 | 0.000 | 61.527 | 13.371 | 94.464 | 1.451 |
| Tetra | 2.083 | 2.151 | 2.151 | 0.000 | 0.000 | 0.000 | 34.847 | 69.993 | 69.993 | 0.000 | 0.000 | 0.000 | 34.847 | 69.993 | 69.993 | 1.498 |
| ⟨100⟩d | 2.656 | 1.971 | 1.971 | 0.000 | 0.000 | 0.000 | 294.306 | -56.839 | -56.839 | 0.000 | 0.000 | 0.000 | 294.306 | -56.839 | -56.839 | 1.547 |
| Octa | 2.002 | 2.002 | 2.616 | 0.000 | 0.000 | 0.000 | -44.451 | -44.451 | 270.159 | 0.000 | 0.000 | 0.000 | -44.451 | -44.451 | 270.159 | 1.553 |
| Vac | -0.501 | -0.501 | -0.501 | 0.000 | 0.000 | 0.000 | -13.726 | -13.726 | -13.726 | 0.000 | 0.000 | 0.000 | -13.726 | -13.726 | -13.726 | -0.353 |

TABLE X. Elements of the dipole tensor $P_{ij}$ (in eV units), the relaxation volume tensor $\Omega_{ij}$ (in Å$^3$ units), eigenvalues of the relaxation volume tensor $\Omega^{(i)}$ (in Å$^3$ units), and the relaxation volume of the defect $\Omega_{rel}$ (in atomic volume units $\Omega_0$) computed for Cs.

| Ba | $P_{11}$ | $P_{22}$ | $P_{33}$ | $P_{12}$ | $P_{23}$ | $P_{31}$ | $\Omega_{11}$ | $\Omega_{22}$ | $\Omega_{33}$ | $\Omega_{12}$ | $\Omega_{23}$ | $\Omega_{31}$ | $\Omega^{(1)}$ | $\Omega^{(2)}$ | $\Omega^{(3)}$ | $\Omega_{rel}$ |
|---|---|---|---|---|---|---|---|---|---|---|---|---|---|---|---|---|
| ⟨111⟩d | 4.098 | 4.098 | 4.098 | 2.226 | 2.226 | 2.226 | 24.611 | 24.611 | 24.611 | 17.171 | 17.171 | 17.171 | 7.440 | 7.440 | 58.953 | 1.162 |
| ⟨111⟩c | 4.083 | 4.083 | 4.083 | 2.260 | 2.260 | 2.260 | 24.519 | 24.519 | 24.519 | 17.432 | 17.432 | 17.432 | 7.087 | 7.087 | 59.382 | 1.157 |
| ⟨110⟩d | 4.061 | 3.822 | 3.822 | 0.000 | 2.176 | 0.000 | 28.805 | 20.742 | 20.742 | 0.000 | 16.786 | 0.000 | 28.805 | 3.956 | 37.527 | 1.106 |
| Tetra | 3.064 | 3.843 | 3.843 | 0.000 | 0.000 | 0.000 | 3.980 | 30.286 | 30.286 | 0.000 | 0.000 | 0.000 | 3.980 | 30.286 | 30.286 | 1.016 |
| ⟨100⟩d | 4.396 | 2.872 | 2.872 | 0.000 | 0.000 | 0.000 | 54.604 | 3.143 | 3.143 | 0.000 | 0.000 | 0.000 | 54.604 | 3.143 | 3.143 | 0.958 |
| Octa | 2.706 | 2.706 | 4.165 | 0.000 | 0.000 | 0.000 | 2.750 | 2.750 | 52.014 | 0.000 | 0.000 | 0.000 | 2.750 | 2.750 | 52.014 | 0.905 |
| Vac | -1.208 | -1.208 | -1.208 | 0.000 | 0.000 | 0.000 | -7.256 | -7.256 | -7.256 | 0.000 | 0.000 | 0.000 | -7.256 | -7.256 | -7.256 | -0.343 |

TABLE XI. Elements of the dipole tensor $P_{ij}$ (in eV units), the relaxation volume tensor $\Omega_{ij}$ (in Å$^3$ units), eigenvalues of the relaxation volume tensor $\Omega^{(i)}$ (in Å$^3$ units), and the relaxation volume of the defect $\Omega_{rel}$ (in atomic volume units $\Omega_0$) computed for Ba.

| V | $P_{11}$ | $P_{22}$ | $P_{33}$ | $P_{12}$ | $P_{23}$ | $P_{31}$ | $\Omega_{11}$ | $\Omega_{22}$ | $\Omega_{33}$ | $\Omega_{12}$ | $\Omega_{23}$ | $\Omega_{31}$ | $\Omega^{(1)}$ | $\Omega^{(2)}$ | $\Omega^{(3)}$ | $\Omega_{rel}$ |
|---|---|---|---|---|---|---|---|---|---|---|---|---|---|---|---|---|
| ⟨111⟩d | 23.140 | 23.140 | 23.140 | -0.029 | -0.029 | -0.029 | 6.578 | 6.578 | 6.578 | -0.086 | -0.086 | -0.086 | 6.664 | 6.664 | 6.406 | 1.472 |
| ⟨111⟩c | 23.143 | 23.143 | 23.143 | -0.081 | -0.081 | -0.081 | 6.579 | 6.579 | 6.579 | -0.244 | -0.244 | -0.244 | 6.822 | 6.822 | 6.092 | 1.473 |
| ⟨110⟩d | 19.264 | 24.929 | 24.929 | 0.000 | -0.003 | 0.000 | 2.152 | 8.748 | 8.748 | 0.000 | -0.009 | 0.000 | 2.152 | 8.757 | 8.739 | 1.466 |
| Tetra | 24.501 | 22.993 | 22.993 | 0.000 | 0.000 | 0.000 | 7.850 | 6.093 | 6.093 | 0.000 | 0.000 | 0.000 | 7.850 | 6.093 | 6.093 | 1.495 |
| ⟨100⟩d | 26.444 | 22.815 | 22.815 | 0.000 | 0.000 | 0.000 | 9.647 | 5.421 | 5.421 | 0.000 | 0.000 | 0.000 | 9.647 | 5.421 | 5.421 | 1.529 |
| Octa | 22.761 | 22.761 | 26.618 | 0.000 | 0.000 | 0.000 | 5.338 | 5.338 | 9.830 | 0.000 | 0.000 | 0.000 | 5.338 | 5.338 | 9.830 | 1.530 |
| Vac | -5.515 | -5.515 | -5.515 | 0.000 | 0.000 | 0.000 | -1.568 | -1.568 | -1.568 | 0.000 | 0.000 | 0.000 | -1.568 | -1.568 | -1.568 | -0.351 |

TABLE XII. Elements of the dipole tensor $P_{ij}$ (in eV units), the relaxation volume tensor $\Omega_{ij}$ (in Å$^3$ units), eigenvalues of the relaxation volume tensor $\Omega^{(i)}$ (in Å$^3$ units), and the relaxation volume of the defect $\Omega_{rel}$ (in atomic volume units $\Omega_0$) computed for V.

| V | $P_{11}$ | $P_{22}$ | $P_{33}$ | $P_{12}$ | $P_{23}$ | $P_{31}$ | $\Omega_{11}$ | $\Omega_{22}$ | $\Omega_{33}$ | $\Omega_{12}$ | $\Omega_{23}$ | $\Omega_{31}$ | $\Omega^{(1)}$ | $\Omega^{(2)}$ | $\Omega^{(3)}$ | $\Omega_{rel}$ |
|---|---|---|---|---|---|---|---|---|---|---|---|---|---|---|---|---|
| ⟨111⟩d | 21.261 | 21.261 | 21.261 | -0.022 | -0.022 | -0.022 | 5.636 | 5.636 | 5.636 | -0.055 | -0.055 | -0.055 | 5.691 | 5.691 | 5.525 | 1.310 |
| ⟨111⟩c | 21.222 | 21.222 | 21.222 | -0.078 | -0.078 | -0.078 | 5.625 | 5.625 | 5.625 | -0.201 | -0.201 | -0.201 | 5.826 | 5.826 | 5.224 | 1.307 |
| ⟨110⟩d | 17.189 | 23.148 | 23.148 | 0.000 | 0.066 | 0.000 | 1.645 | 7.591 | 7.591 | 0.000 | 0.169 | 0.000 | 1.645 | 7.423 | 7.760 | 1.304 |
| Tetra | 22.560 | 20.897 | 20.897 | 0.000 | 0.000 | 0.000 | 6.792 | 5.133 | 5.133 | 0.000 | 0.000 | 0.000 | 6.792 | 5.133 | 5.133 | 1.322 |
| ⟨100⟩d | 24.699 | 20.707 | 20.707 | 0.000 | 0.000 | 0.000 | 8.497 | 4.514 | 4.514 | 0.000 | 0.000 | 0.000 | 8.497 | 4.514 | 4.514 | 1.358 |
| Octa | 20.695 | 20.695 | 24.907 | 0.000 | 0.000 | 0.000 | 4.457 | 4.457 | 8.660 | 0.000 | 0.000 | 0.000 | 4.457 | 4.457 | 8.660 | 1.361 |
| Vac | -7.791 | -7.791 | -7.791 | 0.000 | 0.000 | 0.000 | -2.065 | -2.065 | -2.065 | 0.000 | 0.000 | 0.000 | -2.065 | -2.065 | -2.065 | -0.480 |

TABLE XIII. Elements of the dipole tensor $P_{ij}$ (in eV units), the relaxation volume tensor $\Omega_{ij}$ (in Å$^3$ units), eigenvalues of the relaxation volume tensor $\Omega^{(i)}$ (in Å$^3$ units), and the relaxation volume of the defect $\Omega_{rel}$ (in atomic volume units $\Omega_0$) computed for V using the AM05 exchange-correlation functional.

| Nb | $P_{11}$ | $P_{22}$ | $P_{33}$ | $P_{12}$ | $P_{23}$ | $P_{31}$ | $\Omega_{11}$ | $\Omega_{22}$ | $\Omega_{33}$ | $\Omega_{12}$ | $\Omega_{23}$ | $\Omega_{31}$ | $\Omega^{(1)}$ | $\Omega^{(2)}$ | $\Omega^{(3)}$ | $\Omega_{rel}$ |
|---|---|---|---|---|---|---|---|---|---|---|---|---|---|---|---|---|
| ⟨111⟩d | 30.772 | 30.772 | 30.772 | 2.994 | 2.994 | 2.994 | 9.495 | 9.495 | 9.495 | 12.324 | 12.324 | 12.324 | -2.829 | -2.829 | 34.143 | 1.554 |
| ⟨111⟩c | 30.758 | 30.758 | 30.758 | 2.959 | 2.959 | 2.959 | 9.491 | 9.491 | 9.491 | 12.181 | 12.181 | 12.181 | -2.690 | -2.690 | 33.852 | 1.553 |
| ⟨110⟩d | 29.739 | 30.813 | 30.813 | 0.000 | 1.443 | 0.000 | 8.387 | 9.902 | 9.902 | 0.000 | 5.938 | 0.000 | 8.387 | 3.964 | 15.841 | 1.538 |
| Tetra | 31.916 | 30.687 | 30.687 | 0.000 | 0.000 | 0.000 | 10.752 | 9.017 | 9.017 | 0.000 | 0.000 | 0.000 | 10.752 | 9.017 | 9.017 | 1.571 |
| ⟨100⟩d | 37.069 | 30.512 | 30.512 | 0.000 | 0.000 | 0.000 | 16.259 | 7.005 | 7.005 | 0.000 | 0.000 | 0.000 | 16.259 | 7.005 | 7.005 | 1.651 |
| Octa | 31.153 | 31.153 | 35.689 | 0.000 | 0.000 | 0.000 | 7.945 | 7.945 | 14.347 | 0.000 | 0.000 | 0.000 | 7.945 | 7.945 | 14.347 | 1.650 |
| Vac | -8.805 | -8.805 | -8.805 | 0.000 | 0.000 | 0.000 | -2.717 | -2.717 | -2.717 | 0.000 | 0.000 | 0.000 | -2.717 | -2.717 | -2.717 | -0.445 |

TABLE XIV. Elements of the dipole tensor $P_{ij}$ (in eV units), the relaxation volume tensor $\Omega_{ij}$ (in Å$^3$ units), eigenvalues of the relaxation volume tensor $\Omega^{(i)}$ (in Å$^3$ units), and the relaxation volume of the defect $\Omega_{rel}$ (in atomic volume units $\Omega_0$) computed for Nb.

| Nb | $P_{11}$ | $P_{22}$ | $P_{33}$ | $P_{12}$ | $P_{23}$ | $P_{31}$ | $\Omega_{11}$ | $\Omega_{22}$ | $\Omega_{33}$ | $\Omega_{12}$ | $\Omega_{23}$ | $\Omega_{31}$ | $\Omega^{(1)}$ | $\Omega^{(2)}$ | $\Omega^{(3)}$ | $\Omega_{rel}$ |
|---|---|---|---|---|---|---|---|---|---|---|---|---|---|---|---|---|
| ⟨111⟩d | 31.698 | 31.698 | 31.698 | 3.004 | 3.004 | 3.004 | 9.074 | 9.074 | 9.074 | 10.191 | 10.191 | 10.191 | -1.117 | -1.117 | 29.456 | 1.540 |
| ⟨111⟩c | 31.681 | 31.681 | 31.681 | 2.964 | 2.964 | 2.964 | 9.070 | 9.070 | 9.070 | 10.054 | 10.054 | 10.054 | -0.985 | -0.985 | 29.178 | 1.539 |
| ⟨110⟩d | 30.455 | 31.552 | 31.552 | 0.000 | 1.256 | 0.000 | 8.030 | 9.377 | 9.377 | 0.000 | 4.261 | 0.000 | 8.030 | 5.116 | 13.638 | 1.515 |
| Tetra | 32.739 | 31.201 | 31.201 | 0.000 | 0.000 | 0.000 | 10.338 | 8.450 | 8.450 | 0.000 | 0.000 | 0.000 | 10.338 | 8.450 | 8.450 | 1.541 |
| ⟨100⟩d | 37.685 | 31.168 | 31.168 | 0.000 | 0.000 | 0.000 | 14.879 | 6.878 | 6.878 | 0.000 | 0.000 | 0.000 | 14.879 | 6.878 | 6.878 | 1.620 |
| Octa | 31.823 | 31.823 | 36.123 | 0.000 | 0.000 | 0.000 | 7.761 | 7.761 | 13.040 | 0.000 | 0.000 | 0.000 | 7.761 | 7.761 | 13.040 | 1.616 |
| Vac | -9.175 | -9.175 | -9.175 | 0.000 | 0.000 | 0.000 | -2.627 | -2.627 | -2.627 | 0.000 | 0.000 | 0.000 | -2.627 | -2.627 | -2.627 | -0.446 |

TABLE XV. Elements of the dipole tensor $P_{ij}$ (in eV units), the relaxation volume tensor $\Omega_{ij}$ (in Å$^3$ units), eigenvalues of the relaxation volume tensor $\Omega^{(i)}$ (in Å$^3$ units), and the relaxation volume of the defect $\Omega_{rel}$ (in atomic volume units $\Omega_0$) computed for Nb using the AM05 exchange-correlation functional.

| Mo | $P_{11}$ | $P_{22}$ | $P_{33}$ | $P_{12}$ | $P_{23}$ | $P_{31}$ | $\Omega_{11}$ | $\Omega_{22}$ | $\Omega_{33}$ | $\Omega_{12}$ | $\Omega_{23}$ | $\Omega_{31}$ | $\Omega^{(1)}$ | $\Omega^{(2)}$ | $\Omega^{(3)}$ | $\Omega_{rel}$ |
|---|---|---|---|---|---|---|---|---|---|---|---|---|---|---|---|---|
| ⟨111⟩d | 39.601 | 39.601 | 39.601 | 7.609 | 7.609 | 7.609 | 8.087 | 8.087 | 8.087 | 6.113 | 6.113 | 6.113 | 1.975 | 1.975 | 20.313 | 1.538 |
| ⟨111⟩c | 39.597 | 39.597 | 39.597 | 7.599 | 7.599 | 7.599 | 8.087 | 8.087 | 8.087 | 6.105 | 6.105 | 6.105 | 1.982 | 1.982 | 20.297 | 1.538 |
| ⟨110⟩d | 42.470 | 39.944 | 39.944 | 0.000 | 6.757 | 0.000 | 9.196 | 7.896 | 7.896 | 0.000 | 5.429 | 0.000 | 9.196 | 2.468 | 13.325 | 1.584 |
| Tetra | 37.531 | 43.685 | 43.685 | 0.000 | 0.000 | 0.000 | 6.391 | 9.558 | 9.558 | 0.000 | 0.000 | 0.000 | 6.391 | 9.558 | 9.558 | 1.617 |
| ⟨100⟩d | 48.989 | 40.370 | 40.370 | 0.000 | 0.000 | 0.000 | 11.788 | 7.353 | 7.353 | 0.000 | 0.000 | 0.000 | 11.788 | 7.353 | 7.353 | 1.680 |
| Octa | 39.601 | 39.601 | 50.174 | 0.000 | 0.000 | 0.000 | 6.994 | 6.994 | 12.435 | 0.000 | 0.000 | 0.000 | 6.994 | 6.994 | 12.435 | 1.675 |
| Vac | -9.576 | -9.576 | -9.576 | 0.000 | 0.000 | 0.000 | -1.956 | -1.956 | -1.956 | 0.000 | 0.000 | 0.000 | -1.956 | -1.956 | -1.956 | -0.372 |

TABLE XVI. Elements of the dipole tensor $P_{ij}$ (in eV units), the relaxation volume tensor $\Omega_{ij}$ (in Å$^3$ units), eigenvalues of the relaxation volume tensor $\Omega^{(i)}$ (in Å$^3$ units), and the relaxation volume of the defect $\Omega_{rel}$ (in atomic volume units $\Omega_0$) computed for Mo.

| Mo | $P_{11}$ | $P_{22}$ | $P_{33}$ | $P_{12}$ | $P_{23}$ | $P_{31}$ | $\Omega_{11}$ | $\Omega_{22}$ | $\Omega_{33}$ | $\Omega_{12}$ | $\Omega_{23}$ | $\Omega_{31}$ | $\Omega^{(1)}$ | $\Omega^{(2)}$ | $\Omega^{(3)}$ | $\Omega_{rel}$ |
|---|---|---|---|---|---|---|---|---|---|---|---|---|---|---|---|---|
| ⟨111⟩d | 40.358 | 40.358 | 40.358 | 7.777 | 7.777 | 7.777 | 7.554 | 7.554 | 7.554 | 5.767 | 5.767 | 5.767 | 1.787 | 1.787 | 19.088 | 1.487 |
| ⟨111⟩c | 40.352 | 40.352 | 40.352 | 7.771 | 7.771 | 7.771 | 7.553 | 7.553 | 7.553 | 5.762 | 5.762 | 5.762 | 1.791 | 1.791 | 19.076 | 1.487 |
| ⟨110⟩d | 43.230 | 40.736 | 40.736 | 0.000 | 7.015 | 0.000 | 8.588 | 7.377 | 7.377 | 0.000 | 5.201 | 0.000 | 8.588 | 2.176 | 12.578 | 1.532 |
| Tetra | 38.319 | 44.282 | 44.282 | 0.000 | 0.000 | 0.000 | 5.987 | 8.881 | 8.881 | 0.000 | 0.000 | 0.000 | 5.987 | 8.881 | 8.881 | 1.558 |
| ⟨100⟩d | 49.636 | 41.001 | 41.001 | 0.000 | 0.000 | 0.000 | 11.007 | 6.817 | 6.817 | 0.000 | 0.000 | 0.000 | 11.007 | 6.817 | 6.817 | 1.617 |
| Octa | 40.239 | 40.239 | 50.956 | 0.000 | 0.000 | 0.000 | 6.467 | 6.467 | 11.668 | 0.000 | 0.000 | 0.000 | 6.467 | 6.467 | 11.668 | 1.614 |
| Vac | -10.442 | -10.442 | -10.442 | 0.000 | 0.000 | 0.000 | -1.955 | -1.955 | -1.955 | 0.000 | 0.000 | 0.000 | -1.955 | -1.955 | -1.955 | -0.385 |

TABLE XVII. Elements of the dipole tensor $P_{ij}$ (in eV units), the relaxation volume tensor $\Omega_{ij}$ (in Å$^3$ units), eigenvalues of the relaxation volume tensor $\Omega^{(i)}$ (in Å$^3$ units), and the relaxation volume of the defect $\Omega_{rel}$ (in atomic volume units $\Omega_0$) computed for Mo using the AM05 exchange-correlation functional.

| Ta | $P_{11}$ | $P_{22}$ | $P_{33}$ | $P_{12}$ | $P_{23}$ | $P_{31}$ | $\Omega_{11}$ | $\Omega_{22}$ | $\Omega_{33}$ | $\Omega_{12}$ | $\Omega_{23}$ | $\Omega_{31}$ | $\Omega^{(1)}$ | $\Omega^{(2)}$ | $\Omega^{(3)}$ | $\Omega_{rel}$ |
|---|---|---|---|---|---|---|---|---|---|---|---|---|---|---|---|---|
| ⟨111⟩d | 34.153 | 34.153 | 34.153 | 6.518 | 6.518 | 6.518 | 9.290 | 9.290 | 9.290 | 6.803 | 6.803 | 6.803 | 2.487 | 2.487 | 22.896 | 1.524 |
| ⟨111⟩c | 34.155 | 34.155 | 34.155 | 6.493 | 6.493 | 6.493 | 9.291 | 9.291 | 9.291 | 6.777 | 6.777 | 6.777 | 2.514 | 2.514 | 22.845 | 1.524 |
| ⟨110⟩d | 31.793 | 34.491 | 34.491 | 0.000 | 5.451 | 0.000 | 6.391 | 10.511 | 10.511 | 0.000 | 5.690 | 0.000 | 6.391 | 4.821 | 16.200 | 1.499 |
| Tetra | 34.739 | 34.989 | 34.989 | 0.000 | 0.000 | 0.000 | 9.241 | 9.622 | 9.622 | 0.000 | 0.000 | 0.000 | 9.241 | 9.622 | 9.622 | 1.557 |
| ⟨100⟩d | 42.520 | 33.765 | 33.765 | 0.000 | 0.000 | 0.000 | 18.891 | 5.522 | 5.522 | 0.000 | 0.000 | 0.000 | 18.891 | 5.522 | 5.522 | 1.636 |
| Octa | 34.134 | 34.134 | 42.378 | 0.000 | 0.000 | 0.000 | 5.836 | 5.836 | 18.425 | 0.000 | 0.000 | 0.000 | 5.836 | 5.836 | 18.425 | 1.645 |
| Vac | -10.119 | -10.119 | -10.119 | 0.000 | 0.000 | 0.000 | -2.753 | -2.753 | -2.753 | 0.000 | 0.000 | 0.000 | -2.753 | -2.753 | -2.753 | -0.451 |

TABLE XVIII. Elements of the dipole tensor $P_{ij}$ (in eV units), the relaxation volume tensor $\Omega_{ij}$ (in Å$^3$ units), eigenvalues of the relaxation volume tensor $\Omega^{(i)}$ (in Å$^3$ units), and the relaxation volume of the defect $\Omega_{rel}$ (in atomic volume units $\Omega_0$) computed for Ta.

| Ta | $P_{11}$ | $P_{22}$ | $P_{33}$ | $P_{12}$ | $P_{23}$ | $P_{31}$ | $\Omega_{11}$ | $\Omega_{22}$ | $\Omega_{33}$ | $\Omega_{12}$ | $\Omega_{23}$ | $\Omega_{31}$ | $\Omega^{(1)}$ | $\Omega^{(2)}$ | $\Omega^{(3)}$ | $\Omega_{rel}$ |
|---|---|---|---|---|---|---|---|---|---|---|---|---|---|---|---|---|
| ⟨111⟩d | 34.672 | 34.672 | 34.672 | 6.634 | 6.634 | 6.634 | 8.820 | 8.820 | 8.820 | 6.475 | 6.475 | 6.475 | 2.346 | 2.346 | 21.770 | 1.502 |
| ⟨111⟩c | 34.669 | 34.669 | 34.669 | 6.617 | 6.617 | 6.617 | 8.820 | 8.820 | 8.820 | 6.458 | 6.458 | 6.458 | 2.361 | 2.361 | 21.736 | 1.502 |
| ⟨110⟩d | 32.291 | 34.687 | 34.687 | 0.000 | 5.389 | 0.000 | 6.578 | 9.642 | 9.642 | 0.000 | 5.259 | 0.000 | 6.578 | 4.383 | 14.902 | 1.468 |
| Tetra | 34.868 | 35.361 | 35.361 | 0.000 | 0.000 | 0.000 | 8.533 | 9.164 | 9.164 | 0.000 | 0.000 | 0.000 | 8.533 | 9.164 | 9.164 | 1.525 |
| ⟨100⟩d | 43.261 | 33.980 | 33.980 | 0.000 | 0.000 | 0.000 | 17.345 | 5.475 | 5.475 | 0.000 | 0.000 | 0.000 | 17.345 | 5.475 | 5.475 | 1.606 |
| Octa | 34.482 | 34.482 | 43.268 | 0.000 | 0.000 | 0.000 | 5.771 | 5.771 | 17.009 | 0.000 | 0.000 | 0.000 | 5.771 | 5.771 | 17.009 | 1.621 |
| Vac | -10.703 | -10.703 | -10.703 | 0.000 | 0.000 | 0.000 | -2.723 | -2.723 | -2.723 | 0.000 | 0.000 | 0.000 | -2.723 | -2.723 | -2.723 | -0.464 |

TABLE XIX. Elements of the dipole tensor $P_{ij}$ (in eV units), the relaxation volume tensor $\Omega_{ij}$ (in Å$^3$ units), eigenvalues of the relaxation volume tensor $\Omega^{(i)}$ (in Å$^3$ units), and the relaxation volume of the defect $\Omega_{rel}$ (in atomic volume units $\Omega_0$) computed for Ta using the AM05 exchange-correlation functional.

| W | $P_{11}$ | $P_{22}$ | $P_{33}$ | $P_{12}$ | $P_{23}$ | $P_{31}$ | $\Omega_{11}$ | $\Omega_{22}$ | $\Omega_{33}$ | $\Omega_{12}$ | $\Omega_{23}$ | $\Omega_{31}$ | $\Omega^{(1)}$ | $\Omega^{(2)}$ | $\Omega^{(3)}$ | $\Omega_{rel}$ |
|---|---|---|---|---|---|---|---|---|---|---|---|---|---|---|---|---|
| ⟨111⟩d | 52.754 | 52.754 | 52.754 | 13.128 | 13.128 | 13.128 | 9.209 | 9.209 | 9.209 | 7.402 | 7.402 | 7.402 | 1.808 | 1.808 | 24.012 | 1.712 |
| ⟨111⟩c | 52.745 | 52.745 | 52.745 | 13.151 | 13.151 | 13.151 | 9.207 | 9.207 | 9.207 | 7.414 | 7.414 | 7.414 | 1.793 | 1.793 | 24.036 | 1.711 |
| ⟨110⟩d | 56.960 | 52.557 | 52.557 | 0.000 | 11.277 | 0.000 | 10.908 | 8.693 | 8.693 | 0.000 | 6.358 | 0.000 | 10.908 | 2.335 | 15.050 | 1.753 |
| Tetra | 47.359 | 59.114 | 59.114 | 0.000 | 0.000 | 0.000 | 5.693 | 11.606 | 11.606 | 0.000 | 0.000 | 0.000 | 5.693 | 11.606 | 11.606 | 1.791 |
| ⟨100⟩d | 65.920 | 53.379 | 53.379 | 0.000 | 0.000 | 0.000 | 14.254 | 7.945 | 7.945 | 0.000 | 0.000 | 0.000 | 14.254 | 7.945 | 7.945 | 1.868 |
| Octa | 52.741 | 52.741 | 67.209 | 0.000 | 0.000 | 0.000 | 7.623 | 7.623 | 14.901 | 0.000 | 0.000 | 0.000 | 7.623 | 7.623 | 14.901 | 1.868 |
| Vac | -9.984 | -9.984 | -9.984 | 0.000 | 0.000 | 0.000 | -1.743 | -1.743 | -1.743 | 0.000 | 0.000 | 0.000 | -1.743 | -1.743 | -1.743 | -0.324 |

TABLE XX. Elements of the dipole tensor $P_{ij}$ (in eV units), the relaxation volume tensor $\Omega_{ij}$ (in Å$^3$ units), eigenvalues of the relaxation volume tensor $\Omega^{(i)}$ (in Å$^3$ units), and the relaxation volume of the defect $\Omega_{rel}$ (in atomic volume units $\Omega_0$) computed for W.

| W | $P_{11}$ | $P_{22}$ | $P_{33}$ | $P_{12}$ | $P_{23}$ | $P_{31}$ | $\Omega_{11}$ | $\Omega_{22}$ | $\Omega_{33}$ | $\Omega_{12}$ | $\Omega_{23}$ | $\Omega_{31}$ | $\Omega^{(1)}$ | $\Omega^{(2)}$ | $\Omega^{(3)}$ | $\Omega_{rel}$ |
|---|---|---|---|---|---|---|---|---|---|---|---|---|---|---|---|---|
| ⟨111⟩d | 52.340 | 52.340 | 52.340 | 12.854 | 12.854 | 12.854 | 9.137 | 9.137 | 9.137 | 7.247 | 7.247 | 7.247 | 1.890 | 1.890 | 23.630 | 1.698 |
| ⟨111⟩c | 52.325 | 52.325 | 52.325 | 12.897 | 12.897 | 12.897 | 9.134 | 9.134 | 9.134 | 7.271 | 7.271 | 7.271 | 1.863 | 1.863 | 23.676 | 1.698 |
| ⟨110⟩d | 56.199 | 52.115 | 52.115 | 0.000 | 11.361 | 0.000 | 10.705 | 8.650 | 8.650 | 0.000 | 6.405 | 0.000 | 10.705 | 2.245 | 15.055 | 1.735 |
| Tetra | 45.940 | 59.120 | 59.120 | 0.000 | 0.000 | 0.000 | 5.133 | 11.764 | 11.764 | 0.000 | 0.000 | 0.000 | 5.133 | 11.764 | 11.764 | 1.776 |
| ⟨100⟩d | 65.719 | 52.807 | 52.807 | 0.000 | 0.000 | 0.000 | 14.300 | 7.805 | 7.805 | 0.000 | 0.000 | 0.000 | 14.300 | 7.805 | 7.805 | 1.853 |
| Octa | 51.994 | 51.994 | 67.258 | 0.000 | 0.000 | 0.000 | 7.405 | 7.405 | 15.084 | 0.000 | 0.000 | 0.000 | 7.405 | 7.405 | 15.084 | 1.852 |
| Vac | -10.112 | -10.112 | -10.112 | 0.000 | 0.000 | 0.000 | -1.765 | -1.765 | -1.765 | 0.000 | 0.000 | 0.000 | -1.765 | -1.765 | -1.765 | -0.328 |

TABLE XXI. Elements of elastic dipole tensor $P_{ij}$ (in eV units), the relaxation volume tensor $\Omega_{ij}$ (in Å$^3$ units), eigenvalues of the relaxation volume tensor $\Omega^{(i)}$ (in Å$^3$ units), and the relaxation volume of the defect $\Omega_{rel}$ (in atomic volume $\Omega_0$ units) computed for W. Simulation cells containing defects were relaxed to the stress-free condition.

| W | $P_{11}$ | $P_{22}$ | $P_{33}$ | $P_{12}$ | $P_{23}$ | $P_{31}$ | $\Omega_{11}$ | $\Omega_{22}$ | $\Omega_{33}$ | $\Omega_{12}$ | $\Omega_{23}$ | $\Omega_{31}$ | $\Omega^{(1)}$ | $\Omega^{(2)}$ | $\Omega^{(3)}$ | $\Omega_{rel}$ |
|---|---|---|---|---|---|---|---|---|---|---|---|---|---|---|---|---|
| $\langle 111\rangle$d | 53.843 | 53.843 | 53.843 | 13.218 | 13.218 | 13.218 | 8.689 | 8.689 | 8.689 | 6.738 | 6.738 | 6.738 | 1.952 | 1.952 | 22.164 | 1.669 |
| $\langle 111\rangle$c | 53.843 | 53.843 | 53.843 | 13.243 | 13.243 | 13.243 | 8.689 | 8.689 | 8.689 | 6.750 | 6.750 | 6.750 | 1.939 | 1.939 | 22.190 | 1.669 |
| $\langle 110\rangle$d | 57.374 | 53.705 | 53.705 | 0.000 | 11.768 | 0.000 | 9.958 | 8.318 | 8.318 | 0.000 | 5.999 | 0.000 | 9.958 | 2.319 | 14.316 | 1.703 |
| Tetra | 48.127 | 59.932 | 59.932 | 0.000 | 0.000 | 0.000 | 5.517 | 10.797 | 10.797 | 0.000 | 0.000 | 0.000 | 5.517 | 10.797 | 10.797 | 1.736 |
| $\langle 100\rangle$d | 66.337 | 53.846 | 53.846 | 0.000 | 0.000 | 0.000 | 13.086 | 7.500 | 7.500 | 0.000 | 0.000 | 0.000 | 13.086 | 7.500 | 7.500 | 1.799 |
| Octa | 53.259 | 53.259 | 68.305 | 0.000 | 0.000 | 0.000 | 7.161 | 7.161 | 13.891 | 0.000 | 0.000 | 0.000 | 7.161 | 7.161 | 13.891 | 1.807 |
| Vac | -10.951 | -10.951 | -10.951 | 0.000 | 0.000 | 0.000 | -1.767 | -1.767 | -1.767 | 0.000 | 0.000 | 0.000 | -1.767 | -1.767 | -1.767 | -0.340 |

TABLE XXII. Elements of the dipole tensor $P_{ij}$ (in eV units), the relaxation volume tensor $\Omega_{ij}$ (in Å$^3$ units), eigenvalues of the relaxation volume tensor $\Omega^{(i)}$ (in Å$^3$ units), and the relaxation volume of the defect $\Omega_{rel}$ (in atomic volume units $\Omega_0$) computed for W using the AM05 exchange-correlation functional.

| Cr | $P_{11}$ | $P_{22}$ | $P_{33}$ | $P_{12}$ | $P_{23}$ | $P_{31}$ | $\Omega_{11}$ | $\Omega_{22}$ | $\Omega_{33}$ | $\Omega_{12}$ | $\Omega_{23}$ | $\Omega_{31}$ | $\Omega^{(1)}$ | $\Omega^{(2)}$ | $\Omega^{(3)}$ | $\Omega_{rel}$ |
|---|---|---|---|---|---|---|---|---|---|---|---|---|---|---|---|---|
| $\langle 111\rangle$d | 18.728 | 18.728 | 18.728 | 4.617 | 4.617 | 4.617 | 5.244 | 5.244 | 5.244 | 3.622 | 3.622 | 3.622 | 1.622 | 1.622 | 12.487 | 1.343 |
| $\langle 111\rangle$c | 19.630 | 19.630 | 19.630 | 4.882 | 4.882 | 4.882 | 5.497 | 5.497 | 5.497 | 3.830 | 3.830 | 3.830 | 1.667 | 1.667 | 13.156 | 1.407 |
| $\langle 110\rangle$d | 18.955 | 20.530 | 20.530 | 0.000 | 4.790 | 0.000 | 5.166 | 5.820 | 5.820 | 0.000 | 3.757 | 0.000 | 5.166 | 2.062 | 9.577 | 1.434 |
| Tetra | 16.255 | 25.473 | 25.474 | 0.000 | 0.000 | 0.000 | 3.722 | 7.547 | 7.548 | 0.000 | 0.000 | 0.000 | 3.722 | 7.547 | 7.548 | 1.606 |
| $\langle 100\rangle$d | 29.090 | 19.150 | 19.150 | 0.000 | 0.000 | 0.000 | 9.040 | 4.915 | 4.915 | 0.000 | 0.000 | 0.000 | 9.040 | 4.915 | 4.915 | 1.610 |
| Octa | 17.321 | 17.321 | 32.707 | 0.000 | 0.000 | 0.000 | 4.158 | 4.158 | 10.543 | 0.000 | 0.000 | 0.000 | 4.158 | 4.158 | 10.543 | 1.609 |
| Vac | -5.777 | -5.777 | -5.777 | 0.000 | 0.000 | 0.000 | -1.618 | -1.618 | -1.618 | 0.000 | 0.000 | 0.000 | -1.618 | -1.618 | -1.618 | -0.414 |
| $\langle 11\xi\rangle$d | 18.389 | 18.389 | 21.882 | 4.040 | 2.058 | 2.058 | 4.987 | 4.987 | 6.436 | 3.168 | 1.614 | 1.614 | 1.819 | 4.856 | 9.734 | 1.400 |

TABLE XXIII. Elements of the dipole tensor $P_{ij}$ (in eV units), the relaxation volume tensor $\Omega_{ij}$ (in Å$^3$ units), eigenvalues of the relaxation volume tensor $\Omega^{(i)}$ (in Å$^3$ units), and the relaxation volume of the defect $\Omega_{rel}$ (in atomic volume units $\Omega_0$) computed for Cr.

| Fe | $P_{11}$ | $P_{22}$ | $P_{33}$ | $P_{12}$ | $P_{23}$ | $P_{31}$ | $\Omega_{11}$ | $\Omega_{22}$ | $\Omega_{33}$ | $\Omega_{12}$ | $\Omega_{23}$ | $\Omega_{31}$ | $\Omega^{(1)}$ | $\Omega^{(2)}$ | $\Omega^{(3)}$ | $\Omega_{rel}$ |
|---|---|---|---|---|---|---|---|---|---|---|---|---|---|---|---|---|
| $\langle 111\rangle$d | 23.465 | 23.465 | 23.472 | 5.850 | 5.851 | 5.851 | 6.327 | 6.327 | 6.335 | 4.362 | 4.363 | 4.363 | 1.964 | 1.964 | 15.051 | 1.673 |
| $\langle 111\rangle$c | 23.186 | 23.186 | 23.193 | 5.903 | 5.904 | 5.904 | 6.252 | 6.252 | 6.259 | 4.402 | 4.402 | 4.402 | 1.850 | 1.850 | 15.056 | 1.653 |
| $\langle 110\rangle$d | 25.832 | 21.143 | 21.150 | 0.000 | 5.122 | 0.000 | 9.777 | 4.294 | 4.302 | 0.000 | 3.819 | 0.000 | 9.777 | 0.475 | 8.122 | 1.620 |
| Tetra | 21.396 | 23.331 | 23.339 | 0.000 | 0.001 | 0.000 | 4.607 | 6.871 | 6.880 | 0.000 | 0.000 | 0.000 | 4.607 | 6.871 | 6.880 | 1.619 |
| $\langle 100\rangle$d | 32.284 | 22.931 | 22.937 | 0.000 | 0.000 | 0.000 | 14.316 | 3.378 | 3.385 | 0.000 | 0.000 | 0.000 | 14.316 | 3.378 | 3.385 | 1.858 |
| Octa | 23.273 | 23.273 | 31.302 | 0.000 | 0.000 | 0.000 | 3.869 | 3.869 | 13.258 | 0.000 | 0.000 | 0.000 | 3.869 | 3.869 | 13.258 | 1.851 |
| Vac | -3.081 | -3.081 | -3.081 | 0.000 | 0.000 | 0.000 | -0.831 | -0.831 | -0.831 | 0.000 | 0.000 | 0.000 | -0.831 | -0.831 | -0.831 | -0.220 |

TABLE XXIV. Elements of the dipole tensor $P_{ij}$ (in eV units), the relaxation volume tensor $\Omega_{ij}$ (in Å$^3$ units), eigenvalues of the relaxation volume tensor $\Omega^{(i)}$ (in Å$^3$ units), and the relaxation volume of the defect $\Omega_{rel}$ (in atomic volume units $\Omega_0$) computed for Fe.


[46] A. E. Mattsson and R. Armiento, *Implementing and testing the AM05 spin density functional*, Phys. Rev. B **79**, 155101 (2009).

[47] A. E. Mattsson, R. Armiento R, J. Paier, G. Kresse, J. M. Wills, and T. R. Mattsson, *The AM05 density functional applied to solids*, J. Chem. Phys **128**, 084714 (2008).

[48] R. Hafner, D. Spišák, R. Lorenz and J Hafner, *Magnetic ground state of Cr in density-functional theory*, Phys. Rev. B **65** 184432 (2002)

[49] S. Cottenier, B. De Vries, J. Meersschaut and M. Rots, *What density-functional theory can tell us about the spin-density wave in Cr*, J. Phys.: Condens. Matter **14**, 3275 (2002)

[50] H. C. Herper, E. Hoffmann, and P. Entel, *Ab initio full-potential study of the structural and magnetic phase stability of iron*, Phys. Rev. B **60**, 3839 (1999)

[51] P.-W. Ma, S. L. Dudarev, J. S. Wróbel, *Dynamic simulation of structural phase transitions in magnetic iron*, Phys. Rev. B, **96**, 094418 (2017)

[52] Y. Le Page and P. Saxe, *Symmetry-general least-squares extraction of elastic data for strained materials from ab initio calculations of stress*, Phys. Rev. B **65**, 104104 (2002)

[53] R. P. Feynman, *Forces in Molecules*, Phys. Rev. 56, 340 (1939)

[54] G. Mills, H. Jonsson and G. K. Schenter, *Reversible work transition state theory: application to dissociative adsorp-*

| | $\mathbf{e}^{(1)}$ | $\mathbf{e}^{(2)}$ | $\mathbf{e}^{(3)}$ |
|---|---|---|---|
| $\langle 111 \rangle$d | ( 1 1 -2 ) | ( -1 1 0 ) | ( 1 1 1 ) |
| $\langle 111 \rangle$c | ( 1 1 -2 ) | ( -1 1 0 ) | ( 1 1 1 ) |
| $\langle 110 \rangle$d | ( 1 0 0 ) | ( 0 -1 1 ) | ( 0 1 1 ) |
| Tetra | ( 1 0 0 ) | ( 0 1 0 ) | ( 0 0 1 ) |
| $\langle 100 \rangle$d | ( 1 0 0 ) | ( 0 1 0 ) | ( 0 0 1 ) |
| Octa | ( 1 0 0 ) | ( 0 1 0 ) | ( 0 0 1 ) |
| Vac | ( 1 0 0 ) | ( 0 1 0 ) | ( 0 0 1 ) |
| $\langle 11\xi \rangle$d | ( -1 1 0 ) | ( -0.4893 -0.4893 1 ) | ( 1.0218 1.0218 1 ) |

TABLE XXV. Eigenvectors corresponding to the eigenvalues of the relaxation volume tensor of various defect configurations. Eigenvectors for the relaxation volume tensor of a $\langle 11\xi \rangle$ dumbbell are given only for Cr.

*tion of hydrogen*, Surface Science, **324**, 305 (1995).

[55] H. Jonsson, G. Mills and K. W. Jacobsen, *Nudged Elastic Band Method for Finding Minimum Energy Paths of Transitions*' in *Classical and Quantum Dynamics in Condensed Phase Simulations*, edited by B. J. Berne, G. Ciccotti and D. F. Coker (World Scientific, 1998).

[56] H. C. Nash and C. S. Smith, *Single-crystal elastic constants of lithium*, J. Phys. Chem. Solids **9**, 113 (1959)

[57] C. Kittel, *Introduction to Solid State Physics 7th edition* (John Wiley & Sons, Inc, USA 1996)

[58] R. H. Martinson, *Variation of the Elastic Constants of Sodium with Temperature and Pressure*, Phys. Rev. **178**, 902 (1969)

[59] W. R. Marquardt and J. Trivisonno, *Low temperature elastic constants of potassium*, J. Phys. Chem. Solids **26**, 273 (1965)

[60] E. J. Gutman and J. Trivisonno, *Temperature dependence of the elastic constants of rubidium*, J. Phys. Chem. Solids **28**, 805 (1967)

[61] F. J. Kollarits and J. Trivisonno, *Single-crystal elastic constants of cesium*, J. Phys. Chem. Solids **29**, 2133 (1968)

[62] U. Buchenau, M. Heiroth, H. R. Schober, J. Evers and G. Oehlinger, *Lattice dynamics of strontium and barium*, Phys. Rev. B **30**, 3502 (1984)

[63] M. W. Finnis and J. E. Sinclair, *A simple empirical N-body potential for transition metals*, Phil. Mag. A **50**, 45 (1984)

[64] S. B. Palmer and E. W. Lee, *The elastic constants of chromium*, Phil. Mag. A **24**, 311 (1971)

[65] J. A. Rayne and B. S. Chandrasekhar, *Elastic Constants of Iron from 4.2 to 300K*, Phy. Rev. **122**, 1714 (1961)

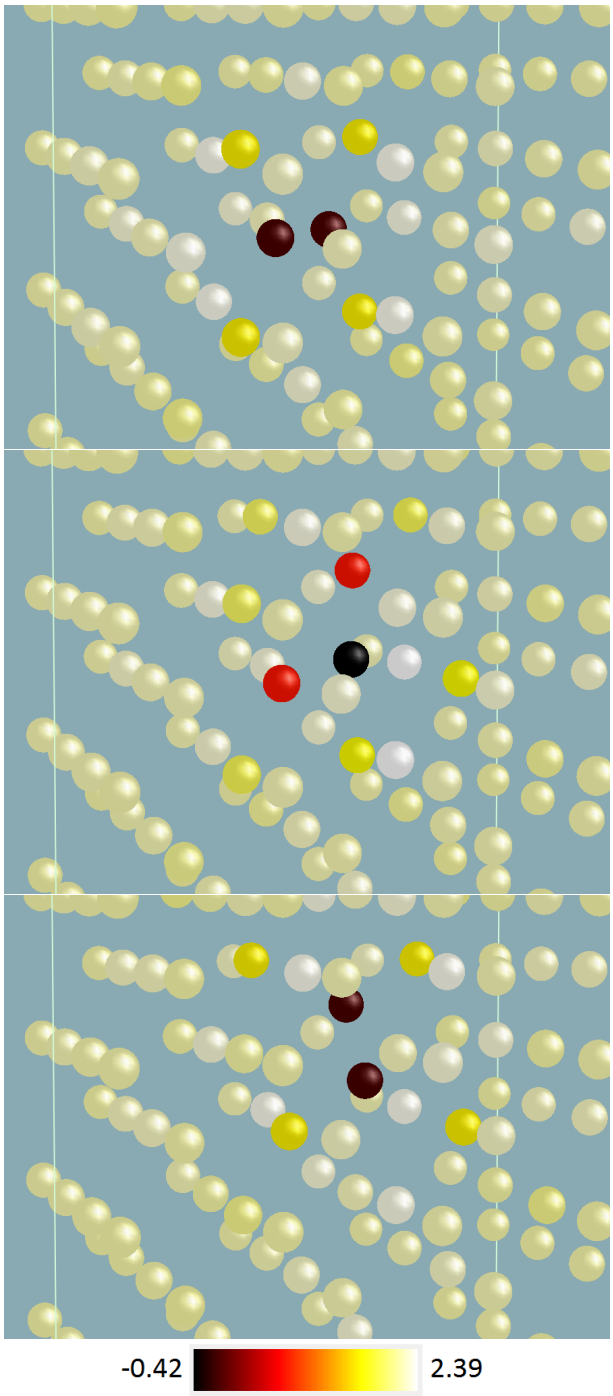


FIG. 6. (Color online) Migration of a ⟨110⟩ dumbbell in Fe. Top: the initial atomic configuration; Middle: the saddle point; Bottom: the final configuration. Colour of atoms refers to the magnitude of atomic magnetic moment given in Bohr magneton units $\mu_B$.

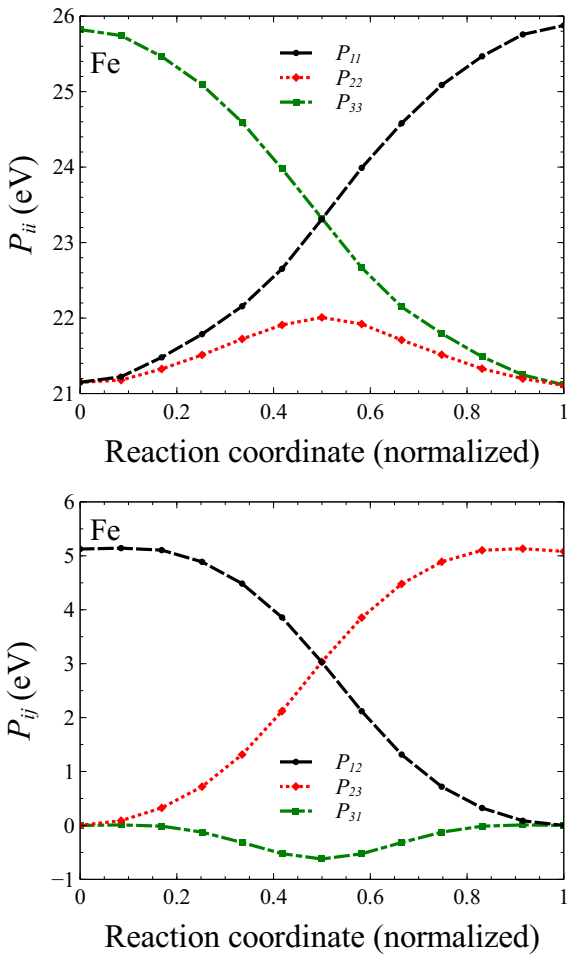


FIG. 7. (Color online) Variation of elements of the dipole tensor of a ⟨110⟩ dumbbell in Fe along the defect migration pathway.

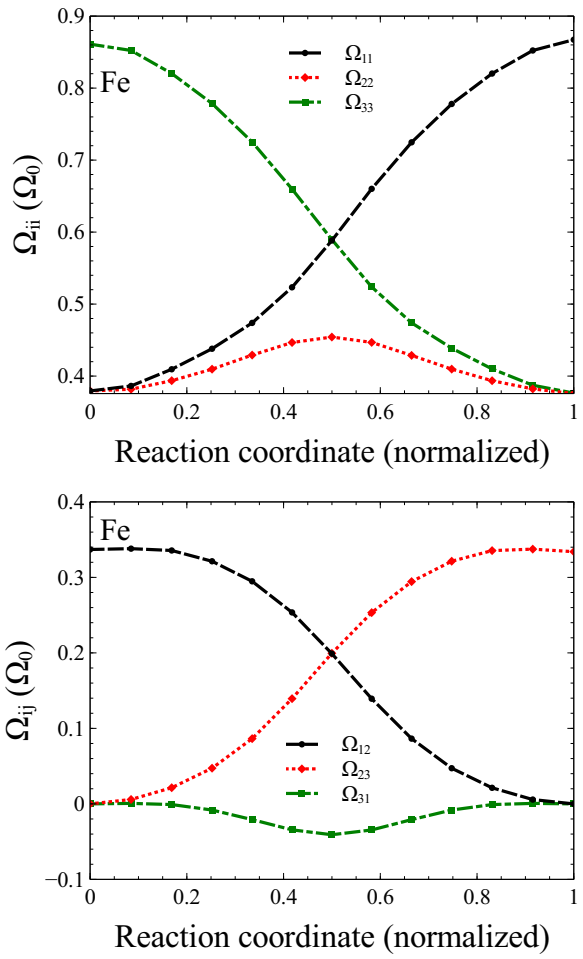


FIG. 8. (Color online) Variation of the relaxation volume tensor of a ⟨110⟩ dumbbell in Fe along the defect migration pathway. The values are given in atomic volume units.